Universiteit Antwerpen

This item is the archived peer-reviewed author-version of:

Dry reforming of methane in a gliding arc plasmatron : towards a better understanding of the plasma chemistry

Reference:
Cleiren Emilie, Heijkers Stijn, Ramakers Marleen, Bogaerts Annemie.- Dry reforming of methane in a gliding arc plasmatron : towards a better understanding of the plasma chemistry
Chemsuschem - ISSN 1864-5631 - 10:20(2017), p. 4025-4036
Full text (Publisher's DOI): https://doi.org/10.1002/CSSC.201701274
To cite this reference: https://hdl.handle.net/10067/1466650151162165141

uantwerpen.be
Institutional repository IRUA

Dry Reforming of Methane in a Gliding Arc Plasmatron: Towards a Better Understanding of the Plasma Chemistry

Emelie Cleiren, Stijn Heijkers, Marleen Ramakers* and Annemie Bogaerts* [a]

Abstract: We studied the dry reforming of methane in a plasma reactor, called gliding arc plasmatron, for different CH_4 fractions in the mixture. The CO_2 and CH_4 conversions reach their highest values of around 18 and 10 %, respectively, at 25 % CH_4 in the gas mixture, corresponding to an overall energy cost of 10 kJ/L (or 2.5 eV/molec) and an energy efficiency of 66 %. CO and H_2 are the major products, with some smaller fractions of C_2H_x (x= 2, 4 or 6) compounds and H_2O formed as well. We also present a chemical kinetics model, to investigate the underlying chemical processes. The calculated CO_2 and CH_4 conversion and the energy efficiency are in good agreement with the experimental data. The model calculations reveal that the reaction of CO_2 (mainly in vibrationally excited levels) with H radicals is mainly responsible for the CO_2 conversion, especially at higher CH_4 fractions in the mixture, and this explains why the CO_2 conversion rises upon rising CH_4 fraction. The main process responsible for CH_4 conversion is the reaction with OH radicals. The excellent energy efficiency can be explained by the non-equilibrium character of the plasma, where the electrons mainly activate the gas molecules, and by the important role of the vibrational kinetics of CO_2. Our results demonstrate that a gliding arc plasmatron is very promising for dry reforming of methane.

Introduction

There is an urgent need to reduce greenhouse gas emissions to avoid further global warming. One possible strategy is to convert CO_2 (and other greenhouse gases, like CH_4) into value added chemicals. In so-called dry reforming of methane (DRM), CO_2 and CH_4 react together, into the formation of syngas (CO/H_2 mixture), hence converting two greenhouse gases simultaneously. Classical catalytic DRM, however, faces some problems, such as the need for high temperatures and catalyst poisoning by carbon deposition. Therefore, in recent years, several novel technologies have been proposed, and one of these is plasma technology.[1,2]

Plasma is a (partially) ionized gas, also called the fourth state of matter. A gas discharge plasma is typically created by applying an electric field to a gas, creating a cocktail of reactive species, such as molecules, radicals, atoms, ions, electrons and excited species, which can all interact with each other, providing the basis for a variety of applications.[3] Plasma technology is of particular interest for energy efficient gas conversion, because the gas must not be heated as a whole for the reactions to take place. Indeed, the electrons are selectively heated by the electric field due to their small mass. These electrons subsequently activate the gas molecules by electron impact excitation, ionization and dissociation, creating reactive species that can easily form new molecules.

Many different types of plasmas have been investigated in recent years for CO_2 conversion, including DRM, and a very recent comprehensive overview is provided in [2], demonstrating the capabilities and limitations of the various plasma types. A gliding arc (GA) plasma is very promising, as it operates at atmospheric pressure and it yields a good energy efficiency, due to the active contribution of the CO_2 vibrational levels in the dissociation process.[4] A classical GA is created by applying a potential difference between two flat diverging electrodes. The arc is created at the shortest interelectrode gap, and is dragged by the gas flow towards larger interelectrode gap, until it

extinguishes and a new arc is again formed at the shortest gap, repeating the cycle. However, a classical GA faces some limitations, like limited gas conversion, because of the short residence time of the gas inside the plasma column.[5-7] Therefore, in recent years, some new designs have been developed, based on cylindrical electrodes and a tangential gas inlet, yielding a vortex flow, so that the gas can stay inside the plasma for a longer time, resulting in a higher conversion. One such type of novel GA is the so-called gliding arc plasmatron (GAP), developed at Drexel University by Nunnally, Rabinovich et al.[8] It has been demonstrated to yield good energy efficiency for pure CO_2 conversion,[8,9] but it was not yet applied for DRM. Other cylindrical (e.g., so-called tornado-type or rotating) GA designs, however, have been applied for DRM already and exhibit very promising results.[10-15]

In this paper, we investigate for the first time the performance of the GAP for DRM. Our experiments will be supported by chemical kinetics modeling to understand the underlying chemical processes. Chemical kinetics modeling is indeed very useful for this purpose, and has been applied to DRM in another type of plasma, i.e., the plasma generated by a dielectric barrier discharge (DBD),[16,17] but not yet by a GA.

Results and Discussion

Measured conversion, energy efficiency and energy cost

We investigated the CO_2 and CH_4 conversion, the energy efficiency and energy cost, as well as the product selectivities (see next section), as a function of the CH_4 fraction in the gas mixture, ranging from 0 to 25 %, for a gas flow rate of 10 L/min. Note that we were limited to a maximum CH_4 fraction of 25 % in the current setup, because the plasma became unstable for larger fractions due to limitations of the power supply. The plasma power is around 500 W in the entire range of CH_4 fractions, yielding a specific energy input (SEI) of ca. 3 kJ/L (or 0.75 eV/molec); see Figure S.1 of the Supporting Information.

Figure 1(a,b) illustrates the measured CO_2 and CH_4 conversion as a function of CH_4 fraction in the mixture. The absolute CO_2 conversion rises from 7.5 to 24 % upon increasing CH_4 fraction, while the absolute CH_4 conversion drops from 61 to 42 %; see Figure 1(a). The CH_4 conversion is much higher than the CO_2 conversion, which can be attributed to the lower bond dissociation energy of C-H (4.48 eV) compared to C=O (5.52 eV), making dissociation of CH_4 easier than for CO_2.

The effective conversion of CO_2 and CH_4 in the mixture is obtained by multiplying the absolute conversion with the fraction of the component in the mixture, and is plotted in Figure 1(b). The effective CO_2 and CH_4 conversion both rise upon increasing CH_4 fraction. Indeed, the rising CH_4 fraction compensates for the lower absolute CH_4 conversion, while the lower CO_2 fraction in the mixture is not important enough to compensate for the higher absolute CO_2 conversion upon adding CH_4 to the mixture. The underlying mechanisms explaining these trends will be discussed later in the paper. As a consequence, the overall conversion also rises upon adding CH_4 to the mixture, from 7.5 to nearly 30 %. These trends agree well with results obtained in a tornado-type GA plasma.[10]

The energy efficiency and energy cost upon rising CH_4 fraction are plotted in Figure 1(c). The energy efficiency more or less follows the rising trend of the overall conversion, while the energy cost follows the opposite trend. This is logical because they are linearly and inversely proportional to the overall conversion, respectively, and they are further determined by the SEI (see formulas 9 and 10 of the Supporting Information) and the latter is more or less constant in the entire range of CH_4 fractions (see Figure S.1 of the Supporting Information). The rising trend in energy efficiency is most striking up to 15 % CH_4 fraction, increasing from 30 % in pure CO_2 to above 60 % between 15 and 25 % CH_4. The energy

cost drops from 37 to 10 kJ/L (or from 9.3 to 2.6 eV/molec) upon rising CH_4 fraction. Note that the trends of rising energy efficiency and decreasing energy cost are accompanied by a slight drop in the temperature of the gas flowing out of the GAP reactor, from 120 °C to 103 °C, at 0 % and 25 % CH_4 fraction, respectively. Obviously, less energy gets lost to gas heating, and more energy can effectively be used for the conversion.

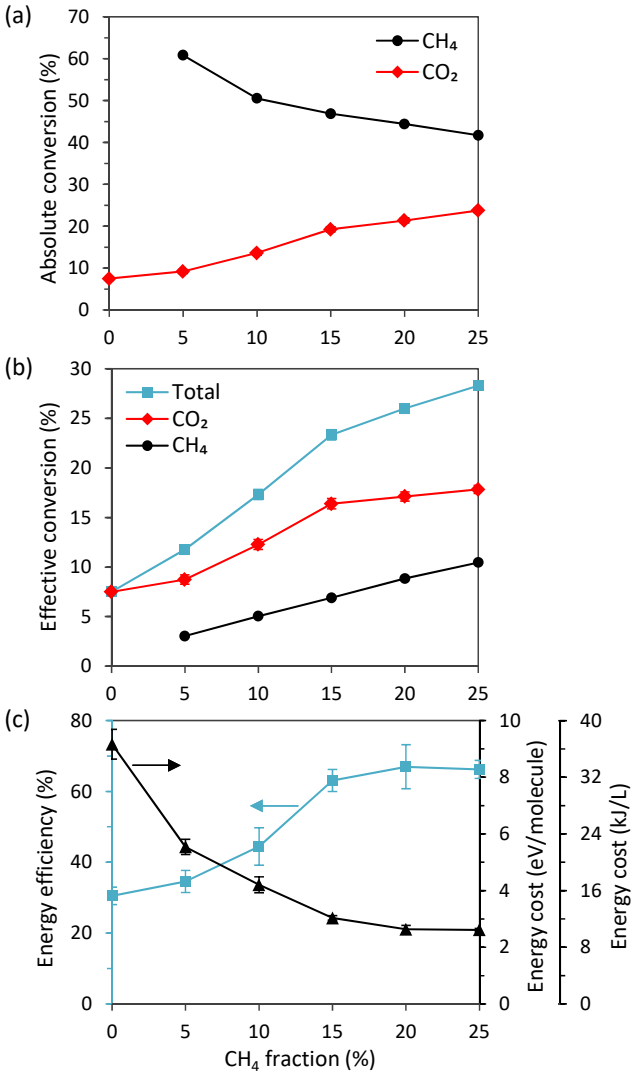

Figure 1. Absolute (a) and effective (b) conversion of CO_2 and CH_4, as well as the total conversion (b), and overall energy efficiency and energy cost (c), as a function of CH_4 fraction in the mixture. The error bars are included in the graphs, but are too small to be visible in (a) and (b).

The combined values of conversion, energy efficiency and energy cost are much better than the typical values obtained in DBDs, which are the most commonly used plasmas for DRM. Indeed, DBDs typically yield maximum conversions of a few % up to 60 % (with a few exceptions up to 80% for packed bed DBDs), but the corresponding energy cost is between 20 and 100 eV/molec (with some lower and higher exceptions for packed bed DBDs).[17-44] Note that we compare with literature values for the energy cost (instead of energy efficiency), because for the latter, one needs to account for all formed products (and their enthalpy of formation; cf. formula 9 in the Supporting Information), and in literature, typically only the selectivity towards the syngas components (and sometimes light hydrocarbons) is reported, making a comparison based on energy efficiencies not very reliable.

Comparison based on the energy cost, however, can provide the same insights in the performance of our GAP compared to other results in literature.

Microwave plasmas are quite promising for pure CO_2 splitting, with energy efficiencies up to 50 % at a conversion up to 26 %,[45,46] but these values are typically reached at reduced pressure, which is less convenient for industrial applications, and the energy cost of vacuum systems would have to be added to the overall energy cost. Moreover, the number of papers on DRM in a MW plasma is very limited. A pulsed MW plasma was able to demonstrate an absolute CH_4 and CO_2 conversion of 71 % and 69 %, respectively, with an energy cost of 6.5 eV/molec.[47] Comparing these results with our GAP, where we obtain an absolute CH_4 and CO_2 conversion up to 61 % and 24 %, respectively (cf. Figure 1(a) above), indicates that the conversion is higher in this MW plasma, but the energy cost is also double the best value reached in our experiments. Another study about a continuous MW plasma yielded similar maximum conversions as in the pulsed MW plasma, but with a higher power (1.5 kW), and thus a very high energy cost up to 343 eV/molec.[48]

For GA plasmas, maximum conversions in the range of 30-50 % have been reported, with energy costs as low as 1-2 eV/molec.[10-15,49-54] The best result reached in literature was obtained for a rotating GA reactor, yielding a total conversion of 39 % with an energy cost of 1 eV/molecule,[11] hence somewhat better than our results.

Other types of plasmas have also been investigated for DRM. In corona discharges, maximum conversions between 10 and 90 % have been reached, with energy cost between 4 and 100 eV/molec.[55-62] The best combined result reported was a conversion of 44 % with an energy cost of 5.2 eV/molec.[56] In spark discharges the minimum energy cost is typically reported around 3-10 eV/molec, for conversions between 10 and 85 %,[63-70] with the best result reporting a total conversion of 85 % with an energy cost of 3.2 eV/molec.[63] Atmospheric pressure glow discharges (APGDs) also seem to be promising for DRM, with maximum conversions of 35-85 % and energy costs of 1-60 eV/molec.[71-73] The best result reported a total conversion of 89 % with an energy cost of only 1.2 eV/molec.[72] Finally, nanosecond-pulsed plasmas provide conversions between 1 and 60 %, for energy costs between 3 and 100 eV/molec.[74-79]

Thus, in general it is clear that the GAP is among the most promising types of plasmas for DRM, in terms of energy cost or energy efficiency. In [2] a maximum energy cost of 4.27 eV/molec, corresponding to a minimum energy efficiency of 60 % (assuming that syngas is the only product formed), was proposed as target for plasma-based DRM to become industrially competitive with classical and other novel conversion technologies. Figure 1(c) illustrates that we reach this target already with our GAP, in case of a sufficient CH_4 fraction in the gas mixture. This good result is attributed to the important role of the vibrational levels of CO_2 for energy efficient conversion, as will be explained later in this paper.

Measured product selectivities

The major products of DRM detected in our GAP are CO, H_2 and (to a much lower extent) O_2, H_2O and C_2H_x hydrocarbons. Our model calculations reveal that other products can also be formed in this gas mixture, as will be discussed below. Figure 2(a) illustrates the (H- and O-based) selectivities of H_2 and O_2 as a function of CH_4 fraction. The remaining H and O atoms will give rise to higher hydrocarbons (C_2H_x) and H_2O, and to CO and H_2O, respectively, and maybe to some minor oxygenated compounds that could not be detected. The strong drop in S_{O,O_2} upon addition of 5 % CH_4 indicates that the O atoms, which are mainly converted into O_2 (and CO) in pure CO_2 splitting, will now be converted into other compounds upon addition of a H-source, so that nearly no O_2 is formed anymore. This will be

discussed in more detail later in the paper. Furthermore, it is clear from Figure 2(a) that the selectivity towards H_2 increases, which is desirable as H_2 is a component of syngas. At low CH_4/CO_2 ratio, the H-based selectivity towards H_2O will be higher.[2]

Figure 2(b) presents the C-based selectivities, as well as the C-balance, which is 100 %. The fact that $S_{C,CO}$ is sometimes higher than the C-balance is probably due to the error associated with this selectivity. It is obvious that CO is the dominant product. The slight drop in $S_{C,CO}$ upon increasing CH_4 fraction is due to a rise in the formation of other C-based products, like C_2-components. The rise in S_{C,C_2} from 2 % to 4 % (see Figure 2(b)) is, however, not sufficient to compensate for the drop of 13 % (with an uncertainty of 6 %) in $S_{C,CO}$, indicating that also other C-based compounds will be formed, which are not detected in our GC.

The two main components formed are thus H_2 and CO (syngas). The H_2/CO ratio rises slightly more than linearly upon increasing CH_4 fraction, from 0.08 at 5 % CH_4 to 0.44 at 25 % CH_4 (see Figure S.2 in the Supporting Information). This is logical, because CH_4 is the only H-source in the mixture. It is clear that the H_2/CO ratio is strongly affected by the gas mixing ratio, and it can be easily tuned by this parameter, to reach optimum values for later Fischer-Tropsch (FT) or methanol synthesis. It should, however, be mentioned that the CO and H_2 yields currently obtained might still be too low for FT or methanol synthesis, which require high yields of CO and H_2 feed gas, as obtained from DRM. This is because the conversion in our current setup is still rather low. In the future, we will try to optimize our setup to improve the conversion (see further).

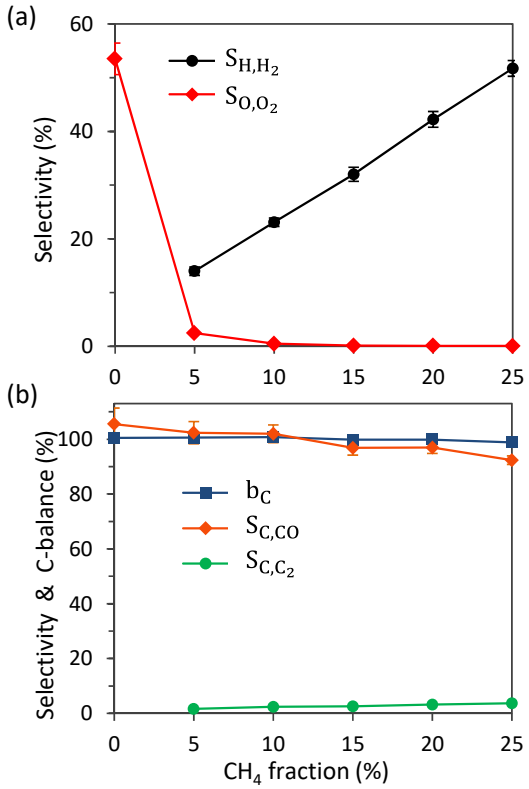

Figure 2. H- and O-based selectivities (a) and C-based selectivities (where C_2 is the sum of C_2H_6, C_2H_4 and C_2H_2) as well as the C-balance (b), as a function of CH_4 fraction in the mixture.

Comparison of measured and calculated conversion and energy efficiency

We developed a chemical kinetics model to investigate the underlying mechanisms of DRM in our GAP, as explained below and in the Supporting Information. Before we can use this model for a deeper analysis, we first need to validate it against the experimental data for conversion and energy efficiency. Figure 3 illustrates the CO_2 (a) and CH_4 (b) conversion as a function of the CH_4 fraction in the mixture, for an input power of 500 W (SEI = 0.75 eV/molec) and gas flow rate of 10 L/min. As explained below, the arc is stabilized in the center of the GAP reactor, and only a fraction of the gas (i.e., 14.8 %; see details below and in the Supporting Information) will pass through this arc column. However, we do not only consider the conversion inside the arc column, but also in a certain region around the actual arc column, which is still at rather high temperature, thus allowing some thermal conversion to take place. Both contributions are indicated in Figure 3 (a,b) with dashed lines. Adding both contributions yields the total conversion, which we can compare with the measured conversion. Both the rising trend in CO_2 conversion (Figure 3(a)) and the drop in CH_4 conversion (Figure 3(b)) are correctly predicted by the model, and also the absolute values are in very good agreement.

It is also clear from Figure 3(a,b) that only accounting for the conversion in the arc column would underestimate the total conversion, especially for CH_4, where the thermal conversion outside the arc column appears to be even higher than the plasma conversion. This is attributed to the lower C-H bond dissociation energy (see above), allowing thermal conversion to occur at lower temperatures. The relative contributions of the conversion inside the arc and the thermal conversion in the area around the arc are plotted for both CO_2 and CH_4 in Figure S.3 of the Supporting Information.

Furthermore, it can be deduced from Figure 3(b) that the CH_4 conversion inside the arc is constant at 14.8 %, independent from the CH_4 fraction in the mixture. The reason is that the CH_4 conversion inside the arc is in fact 100 %, but the overall contribution of the arc is limited by the fraction of gas that passes through the arc, which is predicted to be 14.8 % (see a more detailed discussion below).

Figure 3(c) illustrates the measured and calculated values of the energy efficiency as a function of the CH_4 fraction. Again, the agreement is very good, with relative differences between 1.5 and 27 %, and on average 10 % difference between the values. The rising trend is not exactly the same at low CH_4 fraction, which may indicate that the thermal conversion is somewhat overestimated at 5 (and 10) % CH_4 in the mixture. Indeed, the model simply assumes the same area around the arc column where thermal conversion can take place, but this area will most probably be smaller at low CH_4 fractions, because CH_4 gives rise to a somewhat higher temperature. Obviously, the assumptions made here about the thermal conversion in a fixed area around the arc are a bit rough, due to the inherent nature of the 0D chemical kinetics model. A more accurate description would require full 3D calculations,[80,81] but the latter would result in excessively long calculation times when incorporating the complex CO_2/CH_4 chemistry. Nevertheless, in spite of the approximations that need to be made in the 0D model, the agreement is quite satisfactory.

In general we may conclude that the model provides quite realistic predictions of the CO_2 and CH_4 conversion and of the energy efficiency, so that we can use it to investigate the underlying mechanisms. This will be carried out in the next sections.

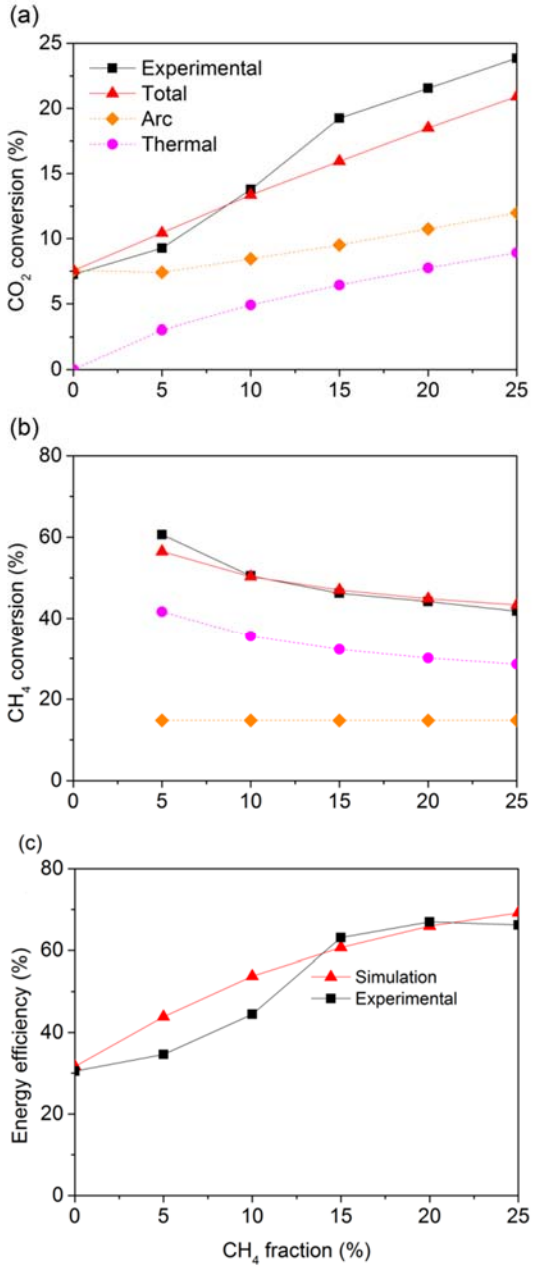

Figure 3. Measured and calculated CO_2 conversion (a) and CH_4 conversion (b), as well as energy efficiency (c) as a function of the CH_4 fraction in the mixture. The individual contributions of the conversion inside the arc and in the thermal area around the arc are indicated in dashed lines in (a) and (b).

Calculated plasma characteristics

Before analyzing the underlying chemical reactions of the CO_2 and CH_4 conversion, we first provide information on the plasma characteristics in the arc column, which help to understand the mechanisms. The important characteristics inside the arc column, defining the plasma chemistry and thus the CO_2 and CH_4 conversion, are the gas temperature, electron temperature and density, and the vibrational temperature, which gives information on the degree of vibrational excitation (see below).

The gas temperature can in principle be calculated in the model (see Supporting Information), but in this study we assume certain values, based on 3D fluid dynamics simulations[80,81] and measured data from literature.[82] Indeed, to obtain realistic calculations with this 0D model, we would need more accurate data on the energy released by some chemical reactions and on the effect of vibration-translation relaxation of the CO_2 vibrational levels upon collision with CH_4, and these data are not

available in literature. Furthermore, the effect of turbulent heat conductivity has also been demonstrated to be very critical in a GAP, yielding a significant drop in gas temperature,[81] and this effect cannot be accounted for in a 0D model.

In Figure 4(a) we plot the assumed gas temperature profile inside the arc column (solid line) and in the thermal area around the arc (dashed line), as a function of position in the reactor. These values are assumed to be independent of the gas mixing ratio, which might be an approximation, but subtle differences for different gas mixtures would lie within the uncertainty of these values. The gas enters the arc column at room temperature, but is quickly heated to about 3500 K after 0.5 cm. The gas in the thermal area around the arc column rises more slowly, up to a value of 2700 K after about 1.2 cm. At this temperature, thermal conversion of CO_2 and CH_4 will indeed take place, as revealed by thermal conversion calculations.[2]

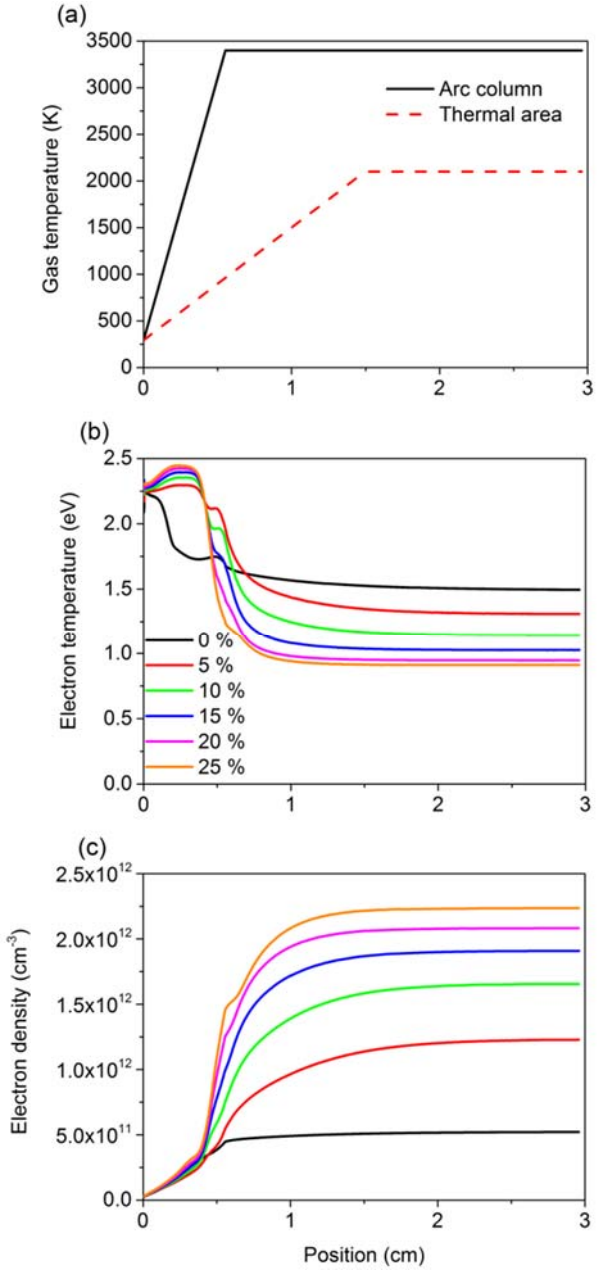

Figure 4. Assumed gas temperature inside the arc column (solid line) and in the thermal area around the arc (dashed line) (a), as well as calculated electron temperature (b) and electron density (c) for different CH_4 fractions in the mixture, as a function of position in the arc. The gas temperature is assumed to be independent from the gas composition.

The calculated electron temperature and density are plotted in Figure 4(b,c) for different CH_4 fractions in the mixture. In the beginning of the arc column the electron density is still low, so that all the applied electrical energy is distributed over a limited number of electrons, explaining the high electron temperature in the beginning of the arc column. This electron temperature is a bit higher than expected for a GA,[1] but it does not really affect the calculated plasma chemistry, because of the low electron density in this region. After about 0.5 cm, the electron density rises, and as a consequence, the electron temperature drops to values of about 1.0 – 1.5 eV (for different CH_4 fractions), which are indeed typical values expected for a GA.[1] The electron temperature slightly drops upon higher CH_4 fraction in the mixture, which is due to the slightly lower values of the reduced electric field (i.e., ratio of electric field over gas density, E/n, typically expressed in Td; 1 Td = 10^{-21} V m²). Indeed, the latter is calculated in the model to be 57 Td and 22 Td, for 0 % and 25 % CH_4 fraction, respectively. Furthermore, a higher CH_4 concentration yields a higher electron density, due to the lower ionisation potential of CH_4 (12.61 eV) vs CO_2 (13.78 eV).

Besides the gas temperature and electron temperature, also the vibrational temperature is an important characteristic of the GAP, because the vibrational levels play a key role in energy efficient CO_2 dissociation. To calculate the vibrational temperature, we plot in Figure 5 the vibrational distribution function (VDF) of the 21 asymmetric mode levels of CO_2 ($v_1 – v_{21}$), as well as the 4 effective symmetric mode levels ($v_a – v_d$; see details about these levels and their notation in the Supporting Information), both inside the arc column and in thermal area around the arc. According to our calculations, the VDF is independent from the CH_4 fraction in the mixture. The faster drop of the VDF for the asymmetric mode levels in the thermal region will yield a somewhat lower vibrational temperature. The latter is a measure for the degree of vibrational excitation, and can be calculated as follows from the VDF, in case of a Boltzmann distribution for the asymmetric mode levels:

$$T_v = \frac{1}{21}\sum_{n=1}^{21}\frac{-E_n}{\ln\left(\frac{n_n}{n_0}\right)} \qquad (1)$$

where E_n is the energy of the n-th asymmetric vibrational level of CO_2, n_n is the density of this level, and n_0 is the density of CO_2 in the ground state.

The vibrational temperature of the asymmetric mode levels is calculated to be about 3400 K inside the arc, and about 2800 K in the thermal area around the arc, which (more or less) corresponds to the gas temperature adopted in both regions. This indicates that the VDF is quasi-thermal. Indeed, no overpopulation of the higher vibrational levels is observed in Figure 5. The same behavior is also seen in a GAP and a classical GA operating in pure CO_2,[5,83-85] as well as in a MW plasma in pure CO_2, when operating at atmospheric pressure.[86] Only in a MW plasma at reduced pressure, an overpopulation of the higher levels was observed,[86-89] because of the less important role of thermalization due to vibration-translation relaxation.

On the other hand, the electron temperature is much higher than the gas temperature and the vibrational temperature (i.e., 1 – 1.55 eV, or 11,000 – 18,000 K vs. 3400 – 3500 K in the arc). This indicates the non-equilibrium character of the GAP, and thus it explains why the CO_2 and CH_4 conversion in the GAP are quite energy efficient, because the electrons are energetic enough to activate the gas by ionization, excitation and dissociation. Nevertheless, if the vibrational temperature would be higher than the gas temperature, due to overpopulation of the higher vibrational levels of CO_2, the CO_2 conversion would still be more energy efficient. A possible way to realize such overpopulation of the higher vibrational levels could be operating at lower gas temperature, in combination with a higher power,[86] or operating at reduced pressure, as demonstrated for MW

plasmas[86-89] (see above). However, the latter is not beneficial for industrial applications, and the cost of the vacuum system would also have to be accounted for in the overall energy efficiency.

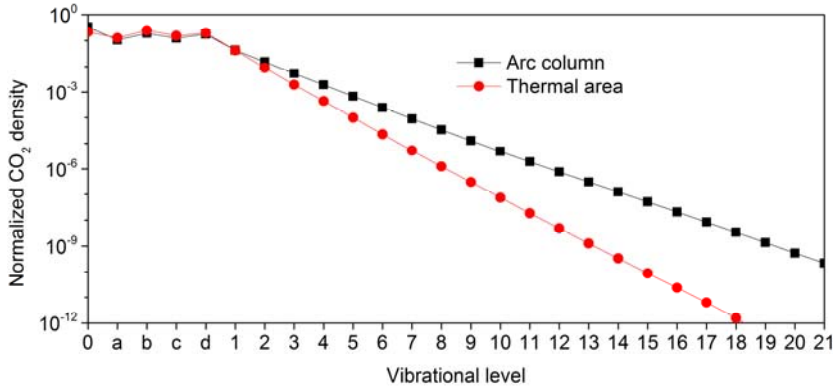

Figure 5. Vibrational distribution functions (VDFs) of all vibrational levels of CO_2 included in the model, both in the arc column and in the thermal area around the arc. These VDFs were found to be the same for all gas mixing ratios investigated. The notations of the vibrational levels are explained in the Supporting Information.

Calculated species densities inside the plasma

In Figure 6 we plot the densities of the most important plasma species at the end of the arc column, as a function of the CH_4 fraction in the mixture. We don't make a distinction between ground state and (vibrationally or electronically excited) levels of the various molecules, and we just plot the sum of both. 84 % of the CO_2 molecules is found in the vibrationally excited levels. For CO, O_2, H_2 and CH_4, this fraction is much lower, i.e., 39 %, 24 %, 4 % and less than 1 %, respectively, and the fraction of electronically excited levels is also of minor importance. For other molecules in the mixture, no vibrational levels are accounted for (see details in Tables S.1 and S.2 in the Supporting Information).

The CO density is higher than the CO_2 density (see Figure 6(a)), indicating that most of the CO_2 is converted inside the arc column. However, for the overall conversion, we also have to account for the fraction of CO_2 gas than cannot pass through the arc column, explaining why the overall conversion is much lower (cf. Figure 3 above). The same applies to the CH_4 density (see Figure 6(b)), which is extremely low, as it is entirely converted to H_2 and higher hydrocarbons inside the arc column. The densities of O_2 and O are only significant in pure CO_2 and they drop considerably upon higher CH_4 fraction in the mixture. This drop was also reflected in the measured O-based selectivity of O_2 (cf. Figure 2 above). Indeed, the O atoms, which recombine into O_2 (and CO) in the pure CO_2 plasma, will now recombine with H atoms, originating from CH_4, into OH, H_2O, CH_3OH and CH_2O, although the densities of the latter species are still quite low (cf. Figure 6(b). The most important products are indeed CO and H_2, along with H_2O. The predominant formation of CO and H_2 could also be deduced from our experimental selectivities (see Figure 2), but the H_2O could not be quantified, due to a very broad band in our GC. Nevertheless, the fact that the sum of the O-based selectivities was not 100 % indicates that a considerable fraction of H_2O will indeed be formed. In addition, oxygenated compounds could be formed, but our model reveals that their densities are much lower. Most probably a catalyst is needed to obtain higher concentrations of these compounds, which we will investigate in the future.

Upon increasing CH_4 fraction in the mixture, more H atoms will be converted into H_2, as is clear from Figure 6(a). Furthermore, Figure 6(b) reveals the following trend for the C_2-compounds:

$C_2H_6 < C_2H_5 < C_2H_4 < C_2H_3 < C_2H_2$

This is in contrast to results observed for a DBD, where C_2H_6 was obtained with the highest concentration of all hydrocarbons, due to recombination of CH_3 radicals.[25] This can probably be explained by the higher temperature in the GAP, leading to more dehydrogenation of C_2H_6, upon electron impact reactions or collisions with O atoms.[49]

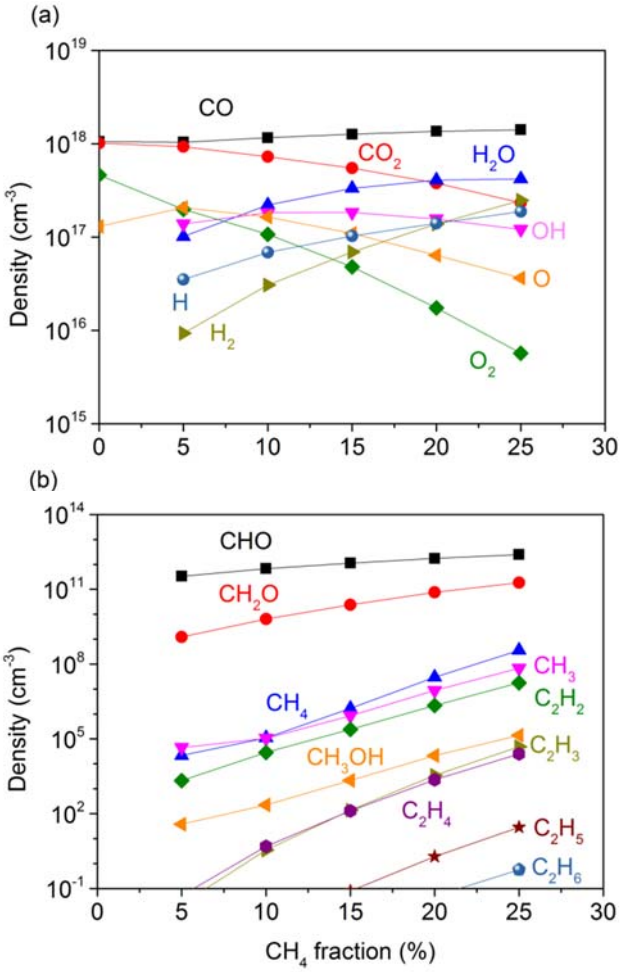

Figure 6. Densities of the most important plasma species at the end of the arc column, as a function of the CH_4 fraction in the mixture.

Chemical kinetics analysis of the underlying processes

The model allows us to obtain a better insight in the loss and formation processes of CO_2 and CH_4, from which we can explain the experimental trends of the CO_2 and CH_4 conversion upon rising CH_4 fraction in the mixture (cf. Figure 1 above). A detailed analysis of these loss and formation processes is presented in the Supporting Information (Figures S.4 – S.7). Based on this analysis, we plot in Figure 7(a,b) the relative contributions of the main processes responsible for the (net) conversion of CO_2 and CH_4, as a function of the CH_4 fraction in the mixture.

Figure 7(a) illustrates that without CH_4 addition, the reaction of CO_2 (mainly in the vibrational levels; see Supporting Information) with either O atoms or any other molecules (indicated as M) is the most important for the conversion of CO_2. The reaction with O atoms becomes dominant at 5 % CH_4 in the mixture, but at larger CH_4 fractions, both processes become less important, while the reaction of CO_2 (again mainly in the vibrational levels; see Supporting Information) with H atoms becomes dominant, with contributions up to 80 % and more. Electron impact dissociation, both from the CO_2 ground state and vibrational levels (see Supporting Information), contributes for about 10 – 20 % to the total CO_2

conversion. It is also clear from Figure S.5 in the Supporting Information that the net CO_2 loss rate rises upon increasing CH_4 fraction, and this is of course attributed to the increasing importance of the reaction with H atoms. Hence, the dissociation of CO_2 upon collision with H atoms explains why the CO_2 conversion rises upon increasing CH_4 fraction in the mixture (cf. Figure 1).

As shown in Figure S.4 of the Supporting Information, the backward reaction of the most important loss process for CO_2 in the CO_2/CH_4 mixture ($CO_2 + H \rightarrow CO + OH$), i.e., the reaction of CO with OH radicals, forming again CO_2 and H atoms, is nearly equally important as the loss (i.e., forward) reaction, especially at low CH_4 fractions. Therefore, this reaction does not contribute to CO_2 conversion at 5% CH_4 in the mixture, and only becomes important at larger CH_4 fractions, as is clear from Figure 7. Note that this backward reaction was also the limiting factor in CO_2 conversion in a DBD operating in a CO_2/H_2O mixture,[90] and it became even more important at higher H_2O fractions in the mixture, explaining why adding H_2O resulted in a drop in the CO_2 conversion.[90] The situation is a bit different in our case, because at higher CH_4 fractions, the H atoms, formed upon dissociation of CH_4, play a more important role in the CO_2 conversion, i.e., the forward (loss) reaction upon collision with H atoms becomes more important than the backward reaction (production of CO_2).

In Figure 7(b) we plot the relative contributions of the net processes contributing to CH_4 conversion, as a function of the CH_4 fraction in the mixture. The reaction of CH_4 with OH radicals is by far the most important, with a contribution of 75 % at low CH_4 fraction, decreasing to 45 % at the highest CH_4 fraction investigated, because of the somewhat lower OH concentration in the mixture (cf. Figure 6(a) above). At the same time, the reaction with C_2H_3 radicals becomes gradually more important, as the density of these radicals rises with increasing CH_4 fraction (cf. Figure 6(b) above). Furthermore, the reaction of CH_4 with H or O atoms, or with C_3H_5 radicals, also plays a minor role, as appears from Figure 7(b). The C_2H_3 and C_3H_5 radicals, as well as the H atoms, of course originate from CH_4. The H atoms are mainly formed by CH_4 dissociation into radicals, while the C_2H_3 and C_3H_5 radicals are mainly formed inside the arc out of CH_2 radicals (created by electron impact dissociation of CH_4) through the following pathways:

$CH_2 + CH_2 \rightarrow C_2H_4$; $C_2H_4 + H \rightarrow C_2H_3 + H_2$

$CH_2 + CH_2 \rightarrow C_2H_2 + 2\,H$; $C_2H_2 + CH_3 \rightarrow C_3H_5$

$C_3H_5 + H + M \rightarrow C_3H_6 + M$; $C_3H_6 \rightarrow C_2H_3 + CH_3$

Besides, in the region near the arc, the following pathways also contribute to the formation of C_2H_3 and C_3H_5 radicals:

$CH_3 + CH_3 \rightarrow C_2H_5 + H$; $C_2H_5 + M \rightarrow C_2H_4 + H + M$;

$C_2H_4 + H \rightarrow C_2H_3 + H_2$

$C_2H_5 + CH_3 \rightarrow C_3H_8 \rightarrow C_3H_7 + H$; $C_3H_7 \rightarrow C_3H_6 + H$;

$C_3H_6 \rightarrow C_3H_5 + H$

Hence, the higher the CH_4 fraction in the mixture, the higher is the effective CH_4 conversion (see Figure 1(b)), and thus the higher is the density of the C_2H_3 and C_3H_5 radicals (see Figure 6(b)), and thus the larger is their contribution to the CH_4 conversion, as can indeed be deduced from Figure 7(b).

Finally, it is clear from Figure S.7 in the Supporting Information that the net CH_4 loss rate rises upon increasing CH_4 fraction. This is mainly due to the increasing CH_4 density in the mixture, and it explains why the measured effective CH_4 conversion rises upon increasing CH_4 fraction (cf. Figure 1(b)). However, the absolute CH_4 conversion drops (cf. Figure 1(a)), and this is mainly attributed to the major loss process, i.e., the reaction of CH_4 with OH radicals, which becomes gradually less important at higher CH_4 fraction in the mixture.

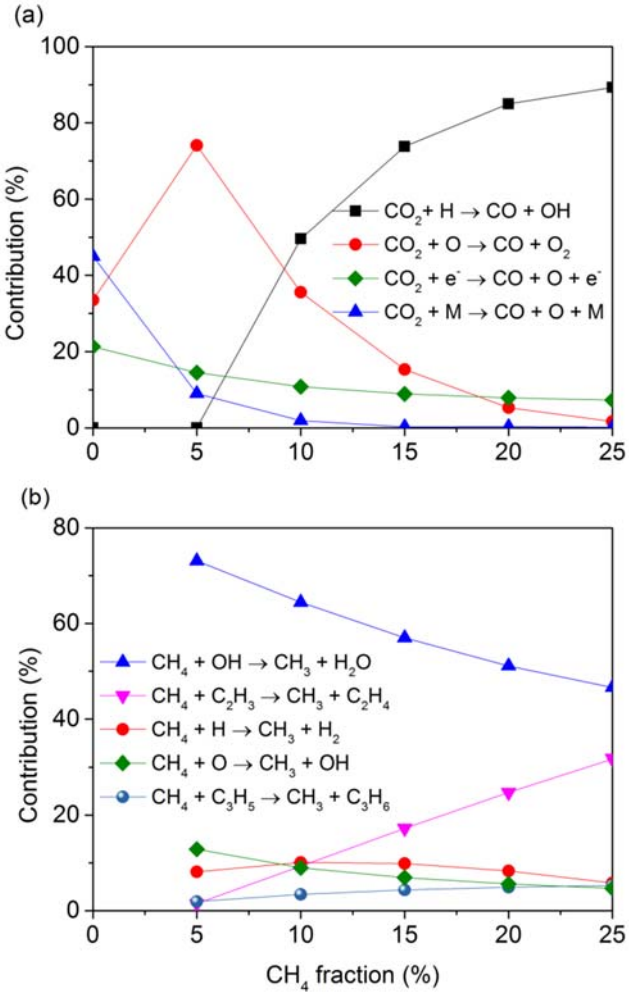

Figure 7. Relative contributions of the main processes responsible for the (net) conversion of CO_2 (a) and CH_4 (b), as a function of CH4 fraction in the mixture.

Conclusions

We present here the dry reforming of methane (DRM) in a gliding arc plasmatron, for different CH_4 fractions in the mixture, by a combination of experiments and chemical kinetics modeling. The CO_2 and CH_4 conversions reach their highest values of around 18 and 10 %, respectively, at 25 % CH_4 in the gas mixture, corresponding to an overall energy cost of 10 kJ/L (or 2.5 eV/molec) and an energy efficiency as high as 66 %. The latter is above the required energy efficiency target, stated in literature to be competitive with classical thermal DRM (i.e., 60 %).[2] CO and H_2 are the major products, with some smaller fractions of C_2H_x compounds formed, as well as H_2O, which could however not be quantified in our GC.

A very good agreement is reached between the measured and calculated conversions and energy efficiency, so we can use the model to elucidate the underlying chemical processes. The model reveals that, besides the conversion inside the arc plasma column, some (thermal) conversion of CO_2 and CH_4 also takes place in the area around the arc column, which is still characterized by relatively high temperature. Inside the arc column, the electron temperature is much higher than the gas temperature, indicating the non-equilibrium character of the plasma, which explains the good energy efficiency of this process. Indeed, the electrons activate the gas molecules by electron impact

excitation, ionization and dissociation, creating reactive species which can more easily form new molecules. The model also demonstrates the important role of the CO_2 vibrational levels. Indeed, most of the CO_2 conversion takes place upon reaction of the CO_2 vibrational levels with radicals from the plasma. The vibrational distribution function (VDF) is, however, in thermal equilibrium with the gas temperature. A higher energy efficiency would still be possible if the higher vibrational levels of CO_2 could be overpopulated, e.g., by operating at low temperatures (in combination with high electric power) or lower pressure.

The CO_2 conversion clearly rises upon increasing CH_4 fraction in the mixture, and this is explained by the model due to the reaction of CO_2 (mainly in vibrationally excited levels) with H atoms, formed upon dissociation of CH_4. The main process responsible for CH_4 conversion is the reaction with OH radicals. Furthermore, reactions with other radicals, such as C_2H_3, H, O and C_3H_5, also play a non-negligible role in the CH_4 conversion.

Our results demonstrate that a gliding arc plasmatron is very promising for DRM, also in comparison with other plasma types, certainly when considering the energy efficiency (or energy cost). The conversion, however, should be further improved. The latter is now limited by the fraction of gas that passes through the plasma column. Indeed, the conversion inside the arc plasma column itself ranges between 51 and 81 % for CO_2 and is already 100 % for CH_4, but a significant fraction of the gas (~ 85 %) does not pass through the plasma column, therefore lowering the overall conversion in the GAP. We believe that we should be able to enhance the gas fraction treated by the arc, by modifying the reactor design (i.e., anode and cathode configuration), enabling the arc to be developed and extend in a larger region of the reactor, or by modifying the gas inlet configuration, enabling a larger gas fraction to pass through the arc. To realize such modifications, more insight is needed in the gas flow dynamics, which is beyond the scope of the present 0D chemical kinetics model, but which we are currently investigating by 2D and 3D fluid dynamics modeling,[80,81] and on which we want to further elaborate in the future, by particle tracing simulations.

Finally, the current experiments were limited to a maximum CH_4 fraction of 25 %, hence well below a stoichiometric mixture of DRM. Indeed, higher CH_4 fractions yielded an unstable plasma due to limitations of the power supply, which was designed for the GAP in pure CO_2. In the future, we would like to perform experiments for larger CH_4 fractions, corresponding to a stoichiometric mixture of DRM, where we expect higher conversions, based on the trend of our current results. The latter would also be necessary if the formed CO/H_2 mixture is further used as feed gas for methanol synthesis or for the FT synthesis of hydrocarbons.

Experimental Section

Description of the experiments

Figure 8 presents a schematic picture of the experimental setup. The GAP consists of two cylindrical electrodes, made of stainless steel (316). The cathode forms the reactor body, while the reactor outlet is at anode potential (see also figure 9 below). The cathode has a diameter of 17.50 mm and a length of 10.20 mm, while the anode length and diameter are 16.30 mm and 7.08 mm, respectively. In addition, the inlet region has a width of 3 mm. This yields a reactor volume of 3.82 cm^3. The setup can be used with different anode diameters, but the present configuration yields the most pronounced reverse vortex flow, as revealed by computational fluid dynamics simulations, providing the best CO_2 conversion and energy efficiency.[9]

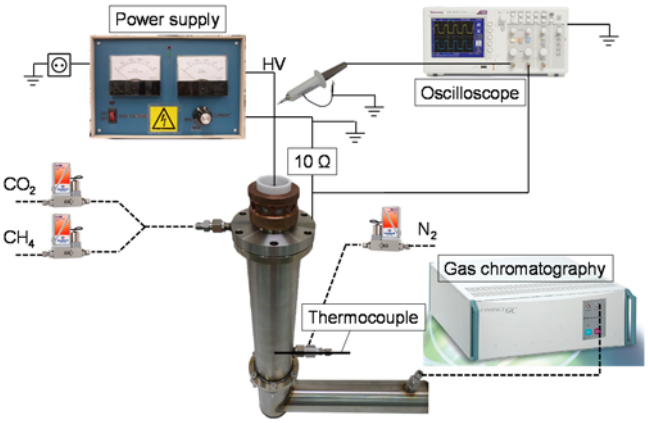

Figure 8. Schematic picture of the experimental setup.

A high voltage (HV) is applied to the GAP, by means of a direct current (DC) power source. The voltage is measured by a high voltage probe (Tektronix P6015A). The current is obtained by measuring the voltage over a resistor of 10 Ohm with a 10x probe. All electrical signals are recorded by a digital oscilloscope with two channels (Tektronix TDS2012C). The current and voltage inside the GAP are 0.27-0.33 A and 0.8-1.0 kV, respectively. The plasma power is calculated from the product of plasma voltage and current over a certain time.

The gas flows in the reactor by six tangential inlets, each with a diameter of 1.6 mm, giving rise to a vortex flow profile. The experiments are performed with a total gas flow rate of 10 L/min, controlled by thermal mass flow controllers (Bronkhorst), and different fractions of CH_4 in the mixture, i.e., 0, 5, 10, 15, 20 and 25 %. The outlet of the GAP is connected to a tube, in which a thermocouple measures the temperature of the outlet gas. The gas is further analyzed in a gas chromatograph (GC). All experiments are carried out in triplicate. Details on the gas analysis, including more information on the gas chromatograph and the way to correct for gas expansion, as well as the formulas to calculate the CO_2 and CH_4 conversion, the product selectivities and energy efficiency and energy cost, are given in the Supporting Information.

Description of the chemical kinetics model

The model presented in this paper is a 0D chemical kinetics model, called ZDPlasKin.[91] It solves the continuity equations for the various plasma species densities, based on production and loss rates:

$$\frac{\mathrm{d}n_i}{\mathrm{d}t} = \sum_j \left[(a_{ij}^R - a_{ij}^L) k_j \prod_l n_l^L \right] \qquad (2)$$

n_i is the density of species i, a_{ij}^R and a_{ij}^L are the stoichiometric coefficients of species i at the left and right hand side of reaction j (R1). n_l is the density of species l at the left hand side of the reaction, and k_j is the reaction rate coefficient of reaction j. Reaction j can in general form be expressed as follows:

$$a_A\mathrm{A} + a_B\mathrm{B}\ (+\delta\varepsilon) \xrightarrow{k_j} a_C\mathrm{C} + a_D\mathrm{D}\ (+\delta\varepsilon) \qquad \text{(R1)}$$

A, B, C, D are the various species, and a_A, a_B, a_C, a_D are their stoichiometric coefficients. $\delta\varepsilon$ represents the energy needed or released by the reaction. More details about the model can be found in the Supporting Information.

In principle, ZDPlasKin can also calculate the gas temperature by a heat conservation equation, but in this work, we apply a certain temperature profile as input in the model, starting from room temperature at the inlet of the arc column, until 3500 K. This is based on 3D fluid dynamics simulations[80,81] and experimental values[82] from literature.

134 different plasma species, including 20 neutral molecules, 37 charged species (i.e., positive and negative ions, as well as the electrons), 24 radicals and 53 excited species, are included in the model. A complete list of these species is given in Table S.1 of the Supporting Information. All these species interact with each other by a large number of chemical reactions, including various (i) electron impact reactions; (ii) electron-ion recombination reactions; (iii) ion-ion, ion-neutral, neutral-neutral reactions; (iv) vibrational-translation (VT) relaxations; and (v) vibrational-vibrational (VV) relaxations.

Application of the 0D model to the GAP

The model is applied to the GAP reactor used for the experiments, considering exactly the same dimensions and operating conditions (gas flow rate of 10 L/min, CH_4 fractions in the mixture ranging from 0 % to 25 %, plasma power of 500 W, corresponding to an SEI of 0.75 eV/molec). A schematic diagram of the GAP, including the dimensions, is presented in Figure 9. The arc plasma column inside the GAP is illustrated by the red rectangle. Because the gas enters the GAP reactor by tangential inlets, it follows a vortex flow pattern. As the outlet (anode) diameter is smaller than the reactor body (cathode part) (see Figure 9), the gas will first move upwards in a so-called forward vortex flow (indicated in Figure 9 by the solid spiral) and when it arrives at the top of the reactor, it will have lost some speed by friction and inertia, so that it will travel downwards in a smaller so-called reverse vortex flow, which is more or less captured by the arc column (see dashed spiral in figure 9). This vortex flow indeed results in stabilization of the arc column in the center of the GAP reactor, as predicted by 3D fluid dynamics modeling. [80,81] Since the plasma confined in the inner vortex gas flow is more or less uniform,[80,81] we can assume a constant power density applied to the gas, during its residence time in the plasma column. Hence, 0D modeling of this kind of plasma is justified. Indeed, the 0D model calculates the species densities as a function of time, and spatial variation by means of transport is not considered. Nevertheless, by means of the gas flow rate, we can convert the temporal variation calculated by the model into a spatial variation in the arc plasma column, and vice versa. The arc plasma column is thus considered as a plug flow reactor, where the plasma characteristics vary as a function of distance travelled by the gas within a certain residence time, in the same way as they would vary as a function of time in a batch reactor.

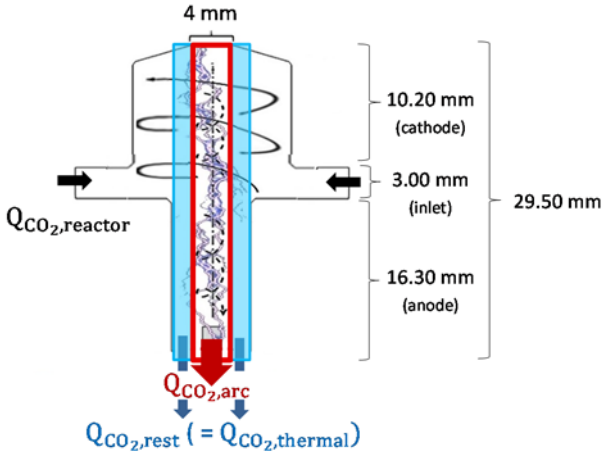

Figure 9. Schematic picture of the GAP, with indication of the dimensions, as well as the outer vortex (solid spiral) and inner (reverse) vortex (dashed spiral). The red frame indicates the arc plasma column, while the blue part indicates the region where thermal conversion takes place.

Calculation of the total CO_2 and CH_4 conversion in the GAP

We can calculate the conversion of CO_2 (as well as of CH_4) after passing through the arc column with the following formula:

$$\chi_{CO_2,arc}(\%) = \left(1 - \frac{n_{CO_2,e} \cdot v_e}{n_{CO_2,i} \cdot v_i}\right) \cdot 100\ \% \qquad (3)$$

n_{CO_2} is the CO_2 density (in m^{-3}) and v is the gas velocity (in m s^{-1}). The indices i and e stand for the values at the beginning of the arc (hence at room temperature) and at the end of the arc (fixed at 3500 K). Because the arc does not fill the entire GAP reactor volume (see Figure 9), not all the gas will be converted by the arc. Hence, to calculate the overall conversion, we have to multiply with the fraction of gas that passes through the arc column, as determined by the fluxes (see Supporting Information). This yields a fraction of 14.8 % of the gas that passes through the arc. The remaining 85.2 % can, however, still be converted thermally in the area around the arc column, which is still characterized by a high temperature (i.e., up to 2700 K; see Figure 4(a)). The conversion in the thermal part ($\chi_{CO_2,thermal}$) is calculated with a similar formula as formula (3). The total CO_2 conversion is then the sum of the conversion inside the arc column ($\chi_{CO_2,arc}$ x 14.8 %) and the thermal conversion in the area around the arc column ($\chi_{CO_2,thermal}$ x 85.2 %). The same applies to the CH_4 conversion. The energy efficiency is determined from the total CO_2 and CH_4 conversion, in the same way as in the experiments (see Supporting Information: Formula 9).

Acknowledgements

We acknowledge financial support from the Fund for Scientific Research – Flanders (FWO; Grant no. G.0383.16N) and the IAP/7 (Inter-university Attraction Pole) program 'PSI-Physical Chemistry of Plasma-Surface Interactions' by the Belgian Federal Office for Science Policy (BELSPO). The calculations were performed using the Turing HPC infrastructure at the CalcUA core facility of the Universiteit Antwerpen, a division of the Flemish Supercomputer Center VSC, funded by the Hercules Foundation, the Flemish Government (department EWI) and the Universiteit Antwerpen. Finally, we would like to thank Georgi Trenchev for the 3D fluid modelling results used as input in the model, and for the assistance in the experiments.

Keywords: CO_2 conversion • Dry reforming • Plasma chemistry • Gliding Arc Plasmatron • Plasma modeling

References

[1] A. Fridman, Plasma Chemistry, Cambridge University Press, New York, 2008.
[2] R. Snoeckx, A. Bogaerts, Chem. Soc. Rev. in press.
[3] A. Bogaerts, E. Neyts, R. Gijbels, J. van der Mullen, Spectrochim. Acta Part B 2002, 57, 609–658.
[4] A. Fridman, A. Chirokov, A. Gutsol, J. Phys. D. Appl. Phys. 2005, 38, R1–R24.
[5] S. R. Sun, H. X. Wang, D. H. Mei, X. Tu, A. Bogaerts, J. CO2 Util. 2017, 17, 220–234.
[6] I. Rusu, J. M. Cormier, Chem. Eng. J. 2003, 91, 23–31.
[7] F. Ouni, A. Khacef, J. M. Cormier, Chem. Eng. Technol. 2006, 29, 604–609.
[8] T. Nunnally, K. Gutsol, A. Rabinovich, A. Fridman, A. Gutsol, A. Kemoun, J. Phys. D 2011, 44, 274009.

[9] M. Ramakers, G. Trenchev, S. Heijkers, W. Wang, A. Bogaerts, ChemSusChem, 2017, 10, 2642-2652.
[10] J. L. Liu, H. W. Park, W. J. Chung, D. W. Park, Plasma Chem. Plasma Process. 2016, 36, 437–449.
[11] A. Wu, J. Yan, H. Zhang, M. Zhang, C. Du, X. Li, Int. J. Hydrogen Energy 2014, 39, 17656–17670.
[12] Z. A. Allah, J. C. Whitehead, Catal. Today 2015, 256, 76–79.
[13] J. L. Liu, H. W. Park, W. J. Chung, W. S. Ahn, D. W. Park, Chem. Eng. J. 2016, 285, 243–251.
[14] K. Li, J. L. Liu, X. Li, X. Zhu, A. Zhu, Chem. Eng. J. 2016, 288, 671–679.
[15] Y. N. Chun, H. W. Song, S. C. Kim, M. S. Lim, Energy Fuels 2008, 22, 123–127.
[16] R. Snoeckx, R. Aerts, X. Tu, A. Bogaerts, J. Phys. Chem. C 2013, 117, 4957–4970.
[17] R. Snoeckx, Y. X. Zeng, X. Tu, A. Bogaerts, RSC Adv. 2015, 5, 29799–29808.
[18] X. Tu, J. C. Whitehead, Appl. Catal. B Environ. 2012, 125, 439–448.
[19] A. Ozkan, T. Dufour, G. Arnoult, P. De Keyzer, A. Bogaerts, F. Reniers, J. CO2 Util. 2015, 9, 78–81.
[20] V. Goujard, J.-M. Tatibouët, C. Batiot-Dupeyrat, Appl. Catal. A Gen. 2009, 353, 228–235.
[21] X. Zhang, M. S. Cha, J. Phys. D. Appl. Phys. 2013, 46, 415205.
[22] Q. Wang, B. H. Yan, Y. Jin, Y. Cheng, Plasma Chem. Plasma Process. 2009, 29, 217–228.
[23] H. K. Song, J. W. Choi, S. H. Yue, H. Lee, B. K. Na, Catal. Today 2004, 89, 27–33.
[24] A. Zhang, A. Zhu, J. Guo, Y. Xu, C. Shi, Chem. Eng. J. 2010, 156, 601–606.
[25] Y. Li, C. J. Liu, B. Eliasson, Y. Wang, Energy Fuels 2002, 16, 864–870.
[26] Y. Zhang, Y. Li, Y. Wang, C. Liu, B. Eliasson, Fuel Process. Technol. 2003, 83, 101–109.
[27] N. R. Pinhão, a. Janeco, J. B. Branco, Plasma Chem. Plasma Process. 2011, 31, 427–439.
[28] H. Song, H. Lee, J.-W. Choi, B. Na, Plasma Chem. Plasma Process. 2004, 24, 57–72.
[29] W. Chung, K. Pan, H. Lee, M. Chang, Energy Fuels 2014, 28, 7621–7631.
[30] Y. Zeng, X. Zhu, D. Mei, B. Ashford, X. Tu, Catal. Today 2015, 256, 80–87.
[31] Q. Wang, Y. Cheng, Y. Jin, Catal. Today 2009, 148, 275–282.
[32] S. Mahammadunnisa, P. M. K. Reddy, B. Ramaraju, C. Subrahmanyam, Energy Fuels 2013, 27, 4441-4447.
[33] X. Zheng, S. Tan, L. Dong, S. Li, H. Chen, J. Power Sources 2015, 274, 286–294.
[34] D. Mei, X. Zhu, C. Wu, B. Ashford, P. T. Williams, X. Tu, Appl. Catal. B Environ. 2016, 182, 17 525–532.
[35] Q. Wang, B. H. Yan, Y. Jin, Y. Cheng, Energy Fuels 2009, 23, 4196–4201.
[36] X. Tu, H. J. Gallon, M. V Twigg, P. A. Gorry, J. C. Whitehead, J. Phys. D. Appl. Phys. 2011, 44, 274007.
[37] X. Zheng, S. Tan, L. Dong, S. Li, H. Chen, Int. J. Hydrogen Energy 2014, 39, 11360–11367.
[38] K. Zhang, T. Mukhriza, X. Liu, P. P. Greco, E. Chiremba, Appl. Catal. A Gen. 2015, 502, 138–149.
[39] M. H. Pham, V. Goujard, J. M. Tatibouët, C. Batiot-Dupeyrat, Catal. Today 2011, 171, 67–71.
[40] J. Sentek, K. Krawczyk, M. Młotek, M. Kalczewska, T. Kroker, T. Kolb, A. Schenk, K. H. Gericke, K. Schmidt-Szałowski, Appl. Catal. B Environ. 2010, 94, 19–26.
[41] K. Krawczyk, M. Młotek, B. Ulejczyk, Fuel 2014, 117, 608–617.
[42] H. J. Gallon, X. Tu, J. C. Whitehead, Plasma Process. Polym. 2012, 9, 90–97.
[43] B. Eliasson, C. Liu, U. Kogelschatz, Ind. Eng. Chem. Res. 2000, 39, 1221–1227.
[44] J. J. Zou, Y. P. Zhang, C. J. Liu, Y. Li, B. Eliasson, Plasma Chem. Plasma Process. 2003, 23, 69–82.
[45] G. J. van Rooij, D. C. M. van den Bekerom, N. den Harder, T. Minea, G. Berden, W. A. Bongers, R. Engeln, M. F. Graswinckel, E. Zoethout, M. C. M. van de Sanden, Faraday Discuss. 2015, 183, 233–248.

[46] W. Bongers, H. Bouwmeester, B. Wolf, F. Peeters, S. Welzel, D. van den Bekerom, N. den Harder, A. Goede, M. Graswinckel, P. W. Groen, et al., Plasma Process. Polym. 2017, 14, e1600126.
[47] J. Q. Zhang, Y. J. Yang, J. S. Zhang, Q. Liu, Acta Chim. Sin. 2002, 60, 1973–1980.
[48] W. Cho, W. S. Ju, S. H. Lee, Y. S. Baek, Y. C. Kim, in Proceedings of 7th International 29 Conference on Carbon Dioxide Utilization 2004, pp. 205–208.
[49] Z. Bo, J. Yan, X. Li, Y. Chi, K. Cen, Int. J. Hydrogen Energy 2008, 33, 5545–5553.
[50] X. Tu, J. C. Whitehead, Int. J. Hydrogen Energy 2014, 39, 9658–9669.
[51] A. Indarto, J. W. Choi, H. Lee, H. K. Song, Energy 2006, 31, 2986–2995.
[52] N. Rueangjitt, C. Akarawitoo, T. Sreethawong, S. Chavadej, Plasma Chem. Plasma Process. 2007, 27, 559–576.
[53] N. Rueangjitt, T. Sreethawong, S. Chavadej, Plasma Chem. Plasma Process. 2008, 28, 49–67.
[54] Y. N. Chun, Y. C. Yang, K. Yoshikawa, Catal. Today 2009, 148, 283–289.
[55] M. Li, C. Liu, Y. Tian, G. Xu, F. Zhang, Y. Wang, Energy Fuels 2006, 20, 1033–1038.
[56] A. Aziznia, H. R. Bozorgzadeh, N. Seyed-matin, M. Baghalha, A. Mohamadalizadeh, J. Nat. Gas Chem. 2012, 21, 466–475.
[57] M. Li, G. Xu, Y. Tian, L. Chen, H. Fu, J. Phys. Chem. A 2004, 108, 1687–1693.
[58] N. Seyed-Matin, A. H. Jalili, M. H. Jenab, S. M. Zekordi, A. Afzali, C. Rasouli, A. Zamaniyan, Plasma Chem. Plasma Process. 2010, 30, 333–347.
[59] M. A. Malik, X. Z. Jiang, Plasma Chem. Plasma Proc. 1999, 19, 505–512.
[60] S. L. Yao, M. Okumoto, A. Nakayama, E. Suzuki, Energy Fuels 2001, 15, 1295–1299.
[61] Y. Yang, Ind. Eng. Chem. Res. 2002, 41, 5918–5926.
[62] C. J. Liu, R. G. Mallinson, L. L. Lobban, Appl. Catal. A Gen. 1999, 178, 17–27.
[63] W. Chung, M. Chang, Energy Convers. Manag. 2016, 124, 305–314.
[64] M. M. Moshrefi, F. Rashidi, H. R. Bozorgzadeh, M. Ehtemam Haghighi, Plasma Chem. Plasma Process. 2013, 33, 453–466.
[65] V. Shapoval, E. Marotta, Plasma Process. Polym. 2015, 12, 808–816.
[66] B. Zhu, X. Li, J. Liu, X. Zhu, A. Zhu, Chem. Eng. J. 2015, 264, 445–452.
[67] X. S. Li, B. Zhu, C. Shi, Y. Xu, A. M. Zhu, AIChE J. 2011, 57, 2854–2860.
[68] S. Kado, K. Urasaki, Y. Sekine, K. Fujimoto, Fuel 2003, 82, 1377–1385.
[69] B. Zhu, X. S. Li, C. Shi, J. L. Liu, T. L. Zhao, A. M. Zhu, Int. J. Hydrogen Energy 2012, 37, 4945–4954.
[70] K. Li, J. Liu, X. Li, X. Zhu, A. Zhu, Catal. Today 2015, 256, 96–101.
[71] A. Huang, G. Xia, J. Wang, S. L. Suib, Y. Hayashi, H. Matsumoto, J. Catal. 2000, 189, 349–359.
[72] D. Li, X. Li, M. Bai, X. Tao, S. Shang, X. Dai, Y. Yin, Int. J. Hydrogen Energy 2009, 34, 308–313.
[73] H. Long, S. Shang, X. Tao, Y. Yin and X. Dai, Int. J. Hydrogen Energy 2008, 33, 5510–5515.
[74] M. Scapinello, L. M. Martini, G. Dilecce, P. Tosi, J. Phys. D. Appl. Phys. 2016, 49, 075602.
[75] A. M. Ghorbanzadeh, S. Norouzi, T. Mohammadi, J. Phys. D Appl. Phys. 2005, 38, 3804–3811.
[76] S. L. Yao, F. Ouyang, A. Nakayama, E. Suzuki, M. Okumoto, A. Mizuno, Energy Fuels 2000, 14, 910–914.
[77] B. Dai, X. L. Zhang, W. M. Gong, R. He, Plasma Sources Sci. Technol. 2000, 2, 577–580.
[78] A. M. Ghorbanzadeh, R. Lotfalipour, S. Rezaei, Int. J. Hydrogen Energy 2009, 34, 293–298.
[79] X. Zhang, B. Dai, A. Zhu, W. Gong, C. Liu, Catal. Today 2002, 72, 223–227.
[80] G. Trenchev, St. Kolev, A. Bogaerts, Plasma Sources Sci. Technol. 2016, 25, 035014.
[81] G. Trenchev, St. Kolev, W. Wang, M. Ramakers, A. Bogaerts, J. CO2 Utiliz. (submitted).
[82] T. Nunnally, Application of Low Current Gliding Arc Plasma Discharges for Hydrogen Sulfide Decomposition and Carbon Dioxide Emission Reduction, Drexel University, 2011.

[83] W. Wang, A. Berthelot, S. Kolev, X. Tu, A. Bogaerts, Plasma Sources Sci. Technol. 2016, 25, 065012.
[84] W. Wang, D. Mei, X. Tu, A. Bogaerts, Chem. Eng. J. (in press).
[85] S. Heijkers, A. Bogaerts, J. Phys. Chem. C. (submitted).
[86] A. Berthelot, A. Bogaerts, J. Phys. Chem. C 2017, 121, 8236-8251.
[87] S. Heijkers, R. Snoeckx, T. Kozák, T. Silva, T. Godfroid, N. Britun, R. Snyders, A. Bogaerts, J. Phys. Chem. C 2015, 119, 12815-12828.
[88] T. Kozák, A. Bogaerts, Plasma Sources Sci. Technol. 2014, 23, 045004.
[89] A. Berthelot, A. Bogaerts, Plasma Sources Sci. Technol. 2016, 25, 045022.
[90] R. Snoeckx, A. Ozkan, F. Reniers, A. Bogaerts, ChemSusChem 2017, 10, 409–424.
[91] S. Pancheshnyi, B. Eismann, G.J.M. Hagelaar, L.C. Pitchford, Computer code ZDPlasKin, http://www.zdplaskin.laplace.univ-tlse.fr (University of Toulouse, LAPLACE, CNRS-UPS-INP, Toulouse, France, 2008).

We investigate the dry reforming of CH_4 in a Gliding Arc Plasmatron, for different CH_4 fractions. We also present a chemical kinetics model, to investigate the underlying chemical processes. It reveals that the reaction of CO_2 with H radicals is responsible for the rising CO_2 conversion upon rising CH_4 fraction. The excellent energy efficiency can be explained by the non-equilibrium character of the plasma, where the electrons mainly activate the gas molecules, and by the important role of the vibrational kinetics of CO_2.

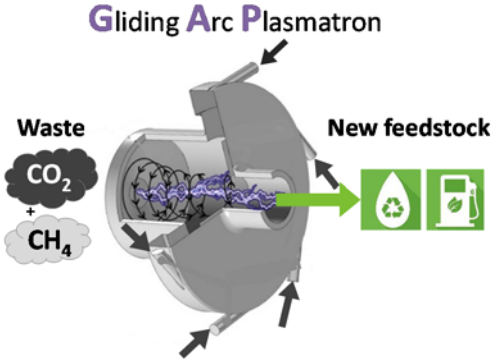

Supporting Information:

Dry Reforming of Methane in a Gliding Arc Plasmatron:

Towards a Better Understanding of the Plasma Chemistry

Emelie Cleiren, Stijn Heijkers, Marleen Ramakers and Annemie Bogaerts

Research group PLASMANT, Department of Chemistry, University of Antwerp

Universiteitsplein 1, BE-2610 Wilrijk-Antwerp, Belgium

E-mail: marleen.ramakers@uantwerpen.be; annemie.Bogaerts@uantwerpen.be

Details on the experiments

Gas analysis

The gas chromatograph used is a compact gas chromatograph (CGC) of Interscience. One measurement takes only 400 s, which is much shorter than for classical GCs. The CGC is equipped with three different ovens, each with a separate column and detector. The first channel has a Rtx-1 column and a flame ionization detector (FID), which can be used to measure alkanes, alkenes and alkynes. The other two channels make use of thermal conductivity detectors (TCDs). The middle channel has two columns, a molecular sieve (Molsieve 5A) and a RT-QBond, and the TCD measures the permanent gases, like O_2, N_2, CO, H_2 and CH_4. The last channel has two RT-QBond columns, which allow the separation of CO_2, lower hydrocarbons (up to C_3), alcohols, aldehydes and ketones.

First a calibration is performed for the compounds to be detected, namely CO_2, CO, O_2, CH_4, H_2, C_2H_2, C_2H_4 and C_2H_6. C_2H_2 and C_2H_4 cannot be separated with the CGC. However, because of their low concentrations (see also Figure 6(b) in the main paper), the C_2-compounds (C_2H_n ; n = 2, 4 or 6) are considered as one compound. H_2O is detected as a broad band, which cannot be quantified. Higher hydrocarbons and oxygenated compounds cannot be detected with this CGC.

Determination of the CO_2 and CH_4 conversion

By analyzing the gas mixture with and without plasma, we can calculate the CO_2 and CH_4 conversions by Formula (1). $C_{i\,(\mathrm{in})}$ and $C_{i\,(\mathrm{out})}$ are the concentrations of component *i* (CO_2 or CH_4) measured after passing through the GAP without plasma (blank measurement) and with plasma, respectively. α is a correction factor, explained in the next section.

$$\chi_i(\%) = \frac{C_{i\,(\mathrm{in})} - \alpha \cdot C_{i\,(\mathrm{out})}}{C_{i(\mathrm{in})}} \cdot 100\ \% \qquad i = CO_2 \text{ or } CH_4 \qquad (1)$$

Besides this (absolute) conversion, we also determine the effective conversion for both CO_2 and CH_4, accounting for the fraction of this component present in the initial gas mixture:

$$\chi_{\mathrm{eff},i}(\%) = \chi_i(\%) \cdot \mathrm{fraction}_i \qquad i = CO_2 \text{ or } CH_4 \qquad (2)$$

The total conversion is the sum of both effective conversions, and is of interest to compare mixtures with different CO_2/CH_4 ratios.

Correction factor for the gas expansion

The correction factor 'α' in Formula (1) accounts for gas expansion taking place during the reaction. Indeed, both in pure CO_2 splitting and dry reforming of methane (DRM), the number of molecules rises

during reaction, so the volumetric flux will rise as well. Because the GC always samples the same volume of the gas flow, neglecting this correction factor, which is done in most papers on plasma-based gas conversion, would overestimate the conversion.[1] Indeed, the sample loop of the GC has a fixed volume, so that gas expansion will yield a pressure rise. However, the GC always samples at atmospheric pressure, so part of the gas will be lost before being injected in the GC. Hence, the number of molecules that will arrive in this sample volume is lower than the original number in the outlet flow. Thus, less molecules will be measured in the sample, which manifests itself as a higher conversion.

To account for this gas expansion, we add an internal standard (N_2) to the outlet gas flow. Using an internal standard has several advantages: (i) it is easy to implement; (ii) no extra calibration is needed; (iii) it has no effect on the reaction processes; (iv) it can be used with every gas mixture.[1]

By comparing the peak surface area of N_2 in the chromatogram with and without plasma, we can obtain the correction factor α (Formula (3))[1] assuming that the ratio of the surface areas is proportional with the ratio of the fluxes.

$$\alpha = \frac{A_{N_2,\text{blank}}}{A_{N_2,\text{plasma}}}(1+\beta) - \beta \tag{3}$$

β is equal to the ratio of the gas flow rate of the internal standard with respect to the total gas flow rate in the GAP (Formula (4)). In this work we always use 10 % of the total gas flow rate as internal standard (β = 0.1), hence for a total gas flow rate of 10 L/min, we add 1 L/min N_2 as internal standard.

$$\beta = \frac{\Phi_{\text{standard}}}{\Phi_{\text{effluent}}} = \frac{\text{gas flow rate}_{N_2}}{\text{gas flow rate}_{CO_2+CH_4}} \tag{4}$$

By adding the internal standard, we need to correct the measured concentrations (C_m) by means of Formula (5) and (6), for the blank measurements and the plasma measurements, respectively.[1]

$$C^{\text{blank}} = C_m^{\text{blank}}(1+\beta) \tag{5}$$

$$C^{\text{plasma}} = C_m^{\text{plasma}}\left(1+\frac{\beta}{\alpha}\right) \tag{6}$$

In the following, we always use the corrected concentrations.

Determination of the specific energy input (SEI), energy efficiency and energy cost

The SEI is calculated from the plasma power and the gas flow rate:

$$\text{SEI (J cm}^{-3}\text{)} = \text{SEI (kJ L}^{-1}\text{)} = \frac{P_{\text{plasma}}\ \text{(kW)}}{\text{gas flow rate (L min}^{-1}\text{)}} \cdot 60\ \text{(s min}^{-1}\text{)} \tag{7}$$

It can also be expressed in eV/molec:

$$\text{SEI (eV molec}^{-1}\text{)} = \frac{\text{SEI (kJ L}^{-1}\text{)} \cdot V_{\text{mol}}\ \text{(L mol}^{-1}\text{)} \cdot 10^3\left(\text{J kJ}^{-1}\right)}{1{,}6.10^{-19}\left(\text{J eV}^{-1}\right) \cdot 6{,}022.\,10^{23}\left(\text{molec mol}^{-1}\right)} \tag{8}$$

V_{mol} is the molar volume, being equal to 22.4 L mol^{-1} (at 0 °C and 1 atm).

The energy efficiency (η) is calculated as follows:

$$\eta = \frac{\alpha \cdot C_{CO(\text{out})} \cdot H_{f,CO} - (\chi_{CH_4} \cdot C_{CH_{4(\text{in})}} \cdot H_{f,CH_4} + \chi_{CO_2} \cdot C_{CO_{2(\text{in})}} \cdot H_{f,CO_2})}{\text{SEI (kJ L}^{-1}\text{)} \cdot V_{\text{mol}}\ \text{(L mol}^{-1}\text{)}} \tag{9}$$

H_f is the enthalpy of formation ($H_{f,CO}$= -110,5 kJ mol^{-1}; H_{f,CH_4}= -74,8 kJ mol^{-1}; H_{f,CO_2}= -393,5 kJ mol^{-1}). The SEI is converted into kJ mol^{-1} by means of the molar volume. This definition yields the chemical energy efficiency. For the sake of completeness, the enthalpy of formation of C_2H_n (n = 2, 4 of 6), and

of other possible (oxygenated) compounds, should be accounted for in the numerator. However, due to the nearly negligible concentrations of these products, these terms can be neglected here.

Finally, the total energy cost (EC) is expressed as:

$$\mathrm{EC_{total}}(\mathrm{eV\ molec^{-1}}) = \frac{\mathrm{SEI\ (eV\ molec^{-1})}}{\chi_{\mathrm{total}}} \tag{10}$$

Determination of the product selectivities and carbon balance

The C-, H- and O-based selectivities of CO, the C_2-based hydrocarbons (C_2H_n ; n = 2, 4 or 6, expressed as C_2), H_2 and O_2, are calculated as follows:

$$\mathrm{S_{C,CO}} = \frac{\alpha \cdot \mathrm{C_{CO(out)}}}{\left(\mathrm{C_{CO_2(in)}} - \alpha \cdot \mathrm{C_{CO_2(out)}}\right) + \left(\mathrm{C_{CH_4(in)}} - \alpha \cdot \mathrm{C_{CH_4(out)}}\right)} \tag{11}$$

$$\mathrm{S_{C,C_2}} = \frac{2 \cdot \alpha \cdot \mathrm{C_{C_2(out)}}}{\left(\mathrm{C_{CO_2(in)}} - \alpha \cdot \mathrm{C_{CO_2(out)}}\right) + \left(\mathrm{C_{CH_4(in)}} - \alpha \cdot \mathrm{C_{CH_4(out)}}\right)} \tag{12}$$

$$\mathrm{S_{H,H_2}} = \frac{\alpha \cdot \mathrm{C_{H_2(out)}}}{2 \cdot \left(\mathrm{C_{CH_4(in)}} - \alpha \cdot \mathrm{C_{CH_4(out)}}\right)} \tag{13}$$

$$\mathrm{S_{O,O_2}} = \frac{\alpha \cdot \mathrm{C_{O_2(out)}}}{\mathrm{C_{CO_2(in)}} - \alpha \cdot \mathrm{C_{CO_2(out)}}} \tag{14}$$

Finally, to determine the ratio of the total number of C atoms in the products vs in the reactant, we calculate the carbon balance:

$$\mathrm{b_C} = \frac{\alpha \cdot \left(\mathrm{C_{CO(out)}} + \mathrm{C_{CO_2(out)}} + \mathrm{C_{CH_4(out)}} + 2 \cdot \mathrm{C_{C_2(out)}}\right)}{\mathrm{C_{CO_2(in)}} + \mathrm{C_{CH_4(out)}}} \tag{15}$$

Details on the computational model

0D model ZDPlasKin

ZDPlasKin (i.e., *Zero-Dimensional Plasma Kinetics solver*)[2] is a Fortran 90 computer code developed to calculate the species densities and the gas temperature as a function of time in non-equilibrium plasmas, by means of conservation equations. The species densities are calculated by continuity equations, based on production and loss rates. A large number of chemical reactions are included. The rate coefficients k_j for reactions between heavy particles are adopted from literature, as a function of gas temperature. The rate coefficients for reactions of electrons depend on the electron energy (and thus on the electron energy distribution function - EEDF), which is defined by the electron temperature or the reduced electric field (i.e., ratio of electric field over gas density; E/n). The latter is calculated by means of a Boltzmann solver (Bolsig+[3]), integrated in ZDPlasKin. This Boltzmann solver solves the Boltzmann equation for electrons, resulting in the EEDF. To solve this equation, we need to know the cross sections of the various elastic and inelastic collisions that can affect the EEDF. These cross sections are adopted from literature.[4-6] The rate coefficients (k_j) for reactions with electrons are calculated as:

$$k_j = \int_0^{+\infty} \sigma_j(\varepsilon) f_e(\varepsilon) \sqrt{\frac{2\varepsilon}{m_e}}\, d\varepsilon \tag{16}$$

ε is the electron energy, $\sigma_j(\varepsilon)$ the cross section of the j-th reaction, $f_e(\varepsilon)$ the EEDF and m_e the mass of an electron (9.1094×10^{-31} kg).

The electric field (E in V.m^{-1}) is calculated by the so-called local field approximation:[7]

$$E = \sqrt{P/\sigma} \tag{17}$$

P is the power density (in W m^{-3}) and σ is the plasma (specific) conductivity (in A V^{-1} m^{-1}), which is estimated in the beginning of the simulation as follows:[7]

$$\sigma = \frac{e^2 \cdot n_{e,init}}{m_e \cdot \nu_m} \tag{18}$$

e is the charge of an electron (1.6022x10^{-19} C), $n_{e,init}$ the initial electron density (in m^{-3}), m_e the mass of an electron (cf. formula (16)) and ν_m the collision frequency (in s^{-1}). The plasma conductivity is updated during the simulations by:[7]

$$\sigma = \frac{e \cdot v_d \cdot n_e}{(E/n)_{previous} \cdot n_0} \tag{19}$$

v_d is the drift velocity of the electrons, calculated with Bolsig+, and $(E/n)_{previous}$ is the reduced electric field in the previous time step.

Finally, the power density, P, is obtained from the arc volume and the plasma power. The latter is simply obtained from the experiments (see main paper and see also Figure S.1 below). The arc volume, however, cannot easily be obtained from the experiments. Nevertheless, based on a 3D fluid plasma model, the movement of the arc in the GAP was simulated,[8] and it was revealed that the arc has a radius of about 1 mm. However, the temperature just outside the arc is still high enough to induce a plasma. Moreover, the 3D simulations were carried out for argon, and we may expect that the temperature outside the arc column is higher for a molecular plasma like CO_2, because of the vibration-translation (VT) relaxations, causing a rise in temperature. Not much is known in literature about the effect of CH_4 on these VT relaxations and the associated heating, but we can safely assume that the arc radius will be larger than 1 mm. In our simulations we assume an arc radius of 2 mm. Combined with the length of the cathode (10.20 mm) and anode (16.30 mm) and the inlet of 3 mm (see Figure 9 of the main paper), this yields a plasma volume of 0.37 cm^3.

Details of the chemistry set

The chemistry set for the conversion of CO_2 and CH_4 (i.e., dry reforming of methane, DRM*)* in our GAP is based on the chemistry set for DRM in a DBD,[6] but extended with the vibrational levels of CO_2. The latter are not included in the chemistry set of the DBD, because vibrationallly excited species have a negligible effect in a DBD, while they are crucial for the dissociation process of CO_2 in a GAP, due to the lower values of the reduced electric field.[9,10] The vibrational levels of CH_4 are limited to the first two levels, because it is known from literature that they have a much smaller population than the vibrational levels of CO_2.[10]

The various plasma species considered in the model are listed in Table S.1. The symbols 'V' and 'E' represent the vibrational and electronic excited levels of CO_2, CO, O_2, CH_4 and H_2. All 21 levels (V_1-V_{21}) of the asymmetric stretch mode of CO_2 (*00n*), up to the dissociation limit of 5.5 eV, are included, because this asymmetric vibrational mode is the most important for energy-efficient dissociation of CO_2.[10] Besides the 21 levels of the asymmetric stretch mode of CO_2, also four (combined) lower lying levels of the symmetric stretch and bending modes are included in the model. Only one electronically excited level of CO_2 (E_1), with a threshold energy of 10.5 eV, is considered, because the other low-lying energy levels immediately give rise to dissociation. The notation, energy and identification of all excited levels is given in Table S.2.

Table S.1: Overview of the species included in the 0D model. An explanation of the notation of the excited species is given in Table S.2.

Neutral molecules	*Charged species*	*Radicals*	*Excited species*
	electrons		
CO_2, CO	CO_2^+, CO_4^+, CO^+, $C_2O_2^+$, $C_2O_3^+$, $C_2O_4^+$, C_2^+, C^+, CO_3^-, CO_4^-	C_2O, C, C_2	CO_2 (V_a, V_b, V_c, V_d), CO_2 (V_1-V_{21}), CO_2 (E_1: 10,5 eV) CO (V_1-V_{10}), CO (E_1-E_4)
O_2, O_3	O^+, O_2^+, O_4^+, O^-, O_2^- O_3^-, O_4^-	O	O_2 (V_1-V_4), O_2 (E_1-E_2)
CH_4	CH_5^+, CH_4^+, CH_3^+, CH_2^+, CH^+	CH_3, CH_2, CH	CH_4 (V_1, V_2)
C_2H_6, C_2H_4, C_2H_2	$C_2H_6^+$, $C_2H_5^+$, $C_2H_4^+$, $C_2H_3^+$, $C_2H_2^+$, C_2H^+	C_2H_5, C_2H_3, C_2H	
C_3H_8, C_3H_6		C_3H_7, C_3H_5	
H_2	H_3^+, H_2^+, H^+, H^-	H	H_2(V_1-V_3), H_2(E_1), H(^{2}P)
H_2O, H_2O_2 CH_2O, CH_3OH, CH_3OOH C_2H_5OH, C_2H_5OOH CH_3CHO, CH_2CO	H_3O^+, H_2O^+, OH^+, OH^-	OH, HO_2 CHO, CH_2OH, CH_3O, CH_3O_2 C_2HO, CH_3CO CH_2CHO, C_2H_5O, $C_2H_5O_2$	

Table S.2: Notation, corresponding energy and identification of the excited levels considered in the model and listed in Table S.1.

	Notation	*Energy (eV)*	*Identification*
Symmetric vibration modes of CO_2	CO_2 (V_a)	0.083	(0 1 0)
	CO_2 (V_b)	0.167	(0 2 0) + (1 0 0)
	CO_2 (V_c)	0.252	(0 3 0) + (1 1 0)
	CO_2 (V_d)	0.339	(0 4 0) + (1 2 0) + (2 0 0)
Asymmetric vibration modes of CO_2	CO_2 (V_1)	0.29	(0 0 1)
	CO_2 (V_2)	0.58	(0 0 2)
	CO_2 (V_3)	0.86	(0 0 3)
	CO_2 (V_4)	1.14	(0 0 4)
	CO_2 (V_5)	1.43	(0 0 5)
	CO_2 (V_6)	1.70	(0 0 6)
	CO_2 (V_7)	1.97	(0 0 7)
	CO_2 (V_8)	2.24	(0 0 8)
	CO_2 (V_9)	2.51	(0 0 9)
	CO_2 (V_{10})	2.77	(0 0 10)
	CO_2 (V_{11})	3.03	(0 0 11)
	CO_2 (V_{12})	3.29	(0 0 12)
	CO_2 (V_{13})	3.55	(0 0 13)

	$CO_2(V_{14})$	3.80	(0 0 14)
	$CO_2(V_{15})$	4.04	(0 0 15)
	$CO_2(V_{16})$	4.29	(0 0 16)
	$CO_2(V_{17})$	4.53	(0 0 17)
	$CO_2(V_{18})$	4.77	(0 0 18)
	$CO_2(V_{19})$	5.01	(0 0 19)
	$CO_2(V_{20})$	5.24	(0 0 20)
	$CO_2(V_{21})$	5.47	(0 0 21)
Electronically excited levels of CO_2	$CO_2(E_1)$	10.5	$^1\Delta_u$
Vibrational levels of CO	$CO(V_1)$	0.266	
	$CO(V_2)$	0.528	
	$CO(V_3)$	0.787	
	$CO(V_4)$	1.040	
	$CO(V_5)$	1.300	
	$CO(V_6)$	1.540	
	$CO(V_7)$	1.790	
	$CO(V_8)$	2.030	
	$CO(V_9)$	2.270	
	$CO(V_{10})$	2.510	
Electronically excited levels of CO	$CO(E_1)$	6.22	$A^3\Pi$
	$CO(E_2)$	7.90	$A^1\Pi$
	$CO(E_3)$	10.4	$A^3\Sigma$, $D^3\Delta$, $E^3\Sigma$, $B^3\Sigma$
	$CO(E_4)$	10.6	$C^1\Sigma$, $E^1\Pi$, $B^1\Sigma$, $I^1\Sigma$, $D^1\Delta$
Vibrational level of O_2	$O_2(V_n)$	0.19 – 0.38 – 0.57 – 0.75	n = 1,…,4
Electronically excited levels of O_2	$O_2(E_1)$	0.98	$A^1\Delta$, $B^1\Sigma$
	$O_2(E_2)$	8.40	$B^3\Sigma$
Vibrational levels of CH_4	$CH_4(V_n)$	0.162 – 0.361	n = 1, 2
Excited levels of H_2 and H	$H_2(V_n)$	0.516 – 1.0 – 1.50	n = 1, 2 ,3
	$H_2(E_1)$	8.9	$B^3\Sigma$
	$H(^2P)$	10.2	

Besides the difference in the importance of the vibrational levels between a DBD and a GAP, also the temperature is greatly different. In contrast to a DBD reactor, which operates (more or less) at room temperature, the temperature in a GAP is much higher (i.e., around 3000-3500 K, according to 3D simulations for argon).[8] Thus, the temperature dependence must be accounted for in the reaction rate coefficients, compared to the DBD chemistry set of [6]. The rate coefficients, including their temperature dependence, are adopted from the NIST database (*National Institute of Standards and Technology Chemical Kinetics Database*).[11]

Calculation of the fraction of gas passing through the arc column

The total gas conversion in the GAP is defined by the conversion inside the arc column, multiplied with the fraction of gas passing through this arc column. In addition, the fraction of gas that does not pass through the arc column, can also thermally be converted, as explained in the main paper.

The total CO_2 conversion by the arc, accounting for the limited fraction of gas passing through the arc, is calculated by:

$$\chi_{CO_2,arc}^{total}(\%) = \left(1 - \frac{Q_{CO_2,arc} + Q_{CO_2,rest}}{Q_{CO_2,reactor}}\right) \cdot 100\ \% \tag{20}$$

$Q_{CO_2,reactor}$, $Q_{CO_2,arc}$ and $Q_{CO_2,rest}$ are the particle fluxes (in s^{-1}) of CO_2 entering the GAP reactor, leaving the arc, and the flux of CO_2 molecules that do not pass through the arc, and will thus not be treated by the plasma. These fluxes are calculated as follows:

$$Q_{CO_2,reactor} = n_{CO_2,i} \cdot \dot{V} \tag{21}$$

$$Q_{CO_2,arc} = n_{CO_2,e} \cdot v_e \cdot A_{arc} \tag{22}$$

$$Q_{CO_2,rest} = Q_{CO_2,reactor} - n_{CO_2,i} \cdot v_i \cdot A_{arc} \tag{23}$$

n_{CO_2} is the CO_2 density (in m^{-3}) and v is the gas velocity (in m s^{-1}). The indices i and e stand for the values at the beginning of the arc (hence at room temperature) and at the end of the arc (fixed at 3500 K). $\dot{V}$ stands for the volumetric gas velocity (m^3 s^{-1}) and A_{arc} is the cross section of the arc column, being equal to 12.57 mm^2 (as the arc radius is 2 mm).

Inserting these fluxes in Formula (20), and using the gas velocity at the beginning of the arc, as obtained from 3D simulations (i.e., 1.96 m/s), yields:

$$\chi_{CO_2,arc}^{total}(\%) = \frac{(n_{CO_2,b} \cdot v_i - n_{CO_2,e} \cdot v_e) \cdot A_{arc}}{n_{CO_2,i} \cdot \dot{V}} \cdot 100\ \%$$

$$\Leftrightarrow$$

$$\chi_{CO_2,arc}^{total}(\%) = \chi_{CO_2,arc}(\%) \cdot \frac{v_i \cdot A_{arc}}{\dot{V}}$$

$$= \chi_{CO_2,arc}(\%) \cdot \frac{1.96\ \text{m s}^{-1}\ \text{x}\ 12.57\text{x}10^{-6}\ \text{m}^2}{10\ \text{x}\ 10^{-3}\ \text{m}^3\ \text{min}^{-1}/(60\ \text{s min}^{-1})}$$

$$= \chi_{CO_2,arc}(\%) \cdot 0.148$$

Note that the same reasoning also applies to CH_4.

Extra information on the experimental results

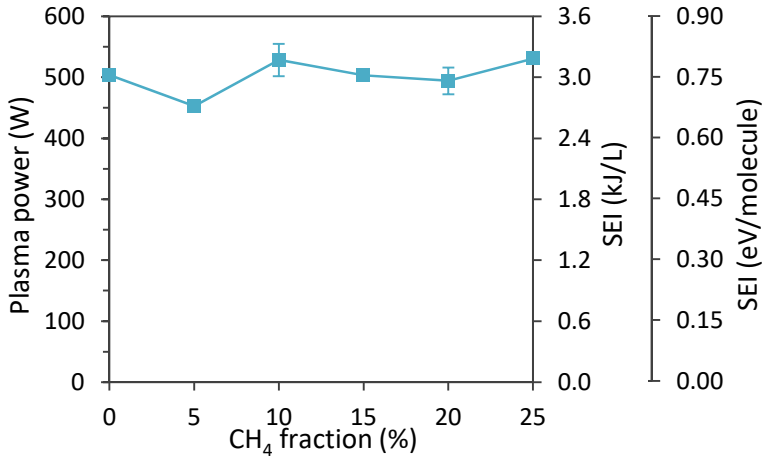

Figure S.1: Plasma power (left axis) and specific energy input (SEI; right axis) as a function of the CH_4 fraction in the mixture, showing that they are more or less constant in the entire gas mixing ratio.

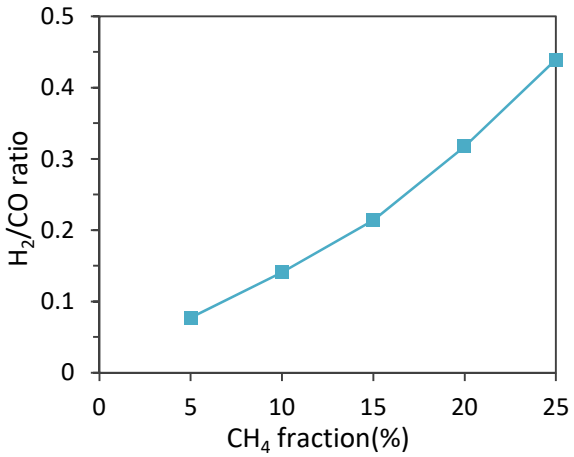

Figure S.2: H_2/CO ratio as a function of the CH_4 fraction in the mixture, showing a slightly more than linear increase.

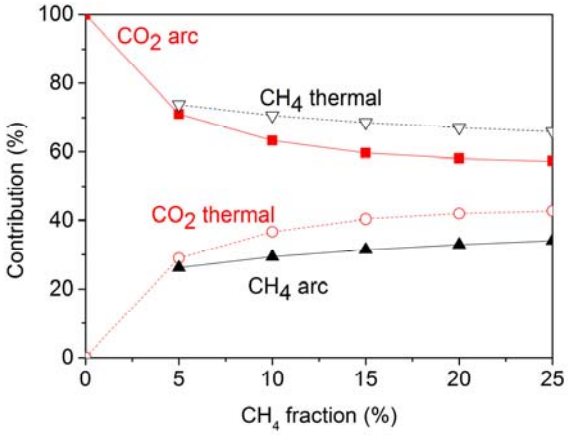

Figure S.3: Relative contribution of the conversion inside the arc and the thermal conversion in the area around the arc to the overall conversion of CO_2 and CH_4, as a function of the CH_4 fraction in the mixture.

Extra information on the calculation results: Detailed analysis of the loss and formation processes of CO_2 and CH_4

Loss and formation of CO_2

Figure S.4 illustrates the time-integrated rates of the major loss (a) and formation (b) processes of CO_2, as a function of the CH_4 fraction in the mixture. The solid lines represent contributions from the vibrationally excited levels of CO_2, while the dashed lines (in the same color) indicate the same reactions from the ground state. It is clear from Figure S.4(a) that the reactions from the CO_2 vibrational levels are more important than those from the ground state, and that the reaction with H atoms (mainly from the vibrational levels, i.e., $CO_2(v) + H \rightarrow CO + OH$; black curve) is by far the dominant loss process. The reactions of $CO_2(v)$ with O atoms or any molecule M (red and blue curve) are only important at low CH_4 fractions, where the H atom density is still low, and the O atom density is still high (cf. also Figure 6(a) from the main paper). Indeed, in the CO_2/CH_4 mixture, the O atoms will react with CH_4 (and dissociation products, like H atoms), to form OH (and CH_3) radicals, so their contribution in CO_2 splitting drops.

In spite of the fact that the reaction of CO_2 with H atoms is by far the dominant one, its opposite reaction (i.e., $CO + OH \rightarrow CO_2 + H$) is nearly equally important, as shown in Figure S.4(b). The same applies, to a lower extent, for the opposite reactions of the collisions with O atoms or molecules M (cf. red and blue curves in Figures S.4(b)). Therefore, we need to look at the time-integrated rates of the net reactions (i.e., forward minus reverse reaction of the same kind) and they are plotted in Figure S.5. The same colors are used as in Figure S.4, for the sake of clarity. Furthermore, the total (time-integrated) net loss rate is also plotted. Note that the rates of the net loss reactions are plotted as negative values, while the net production reaction rates would occur as positive values. It is, however, clear from Figure S.5 that there is a net loss of CO_2, for all gas mixing ratios investigated, and the loss rate rises with increasing CH_4 fraction in the mixture. This explains the higher CO_2 conversion upon higher CH_4 fraction in the mixture. The reaction of CO_2 with H atoms is the most important net loss process, except at low CH_4 fractions, where reactions with O atoms or molecules M are more important, but their contribution drops upon rising CH_4 fraction. The fact that the net rate of the reaction with O atoms rises at 5 % CH_4 fraction is because the rate of the opposite reaction ($CO + O_2 \rightarrow CO_2 + O$) drops faster than the rate of the forward reaction ($CO_2 + O \rightarrow CO + O_2$) upon addition of CH_4. However, at larger CH_4 fractions, the rate of the forward reaction also drops due to the lower O atom density in the plasma. Finally, the contribution of electron impact dissociation is not negligible, and seems to be independent from the CH_4 fraction in the mixture.

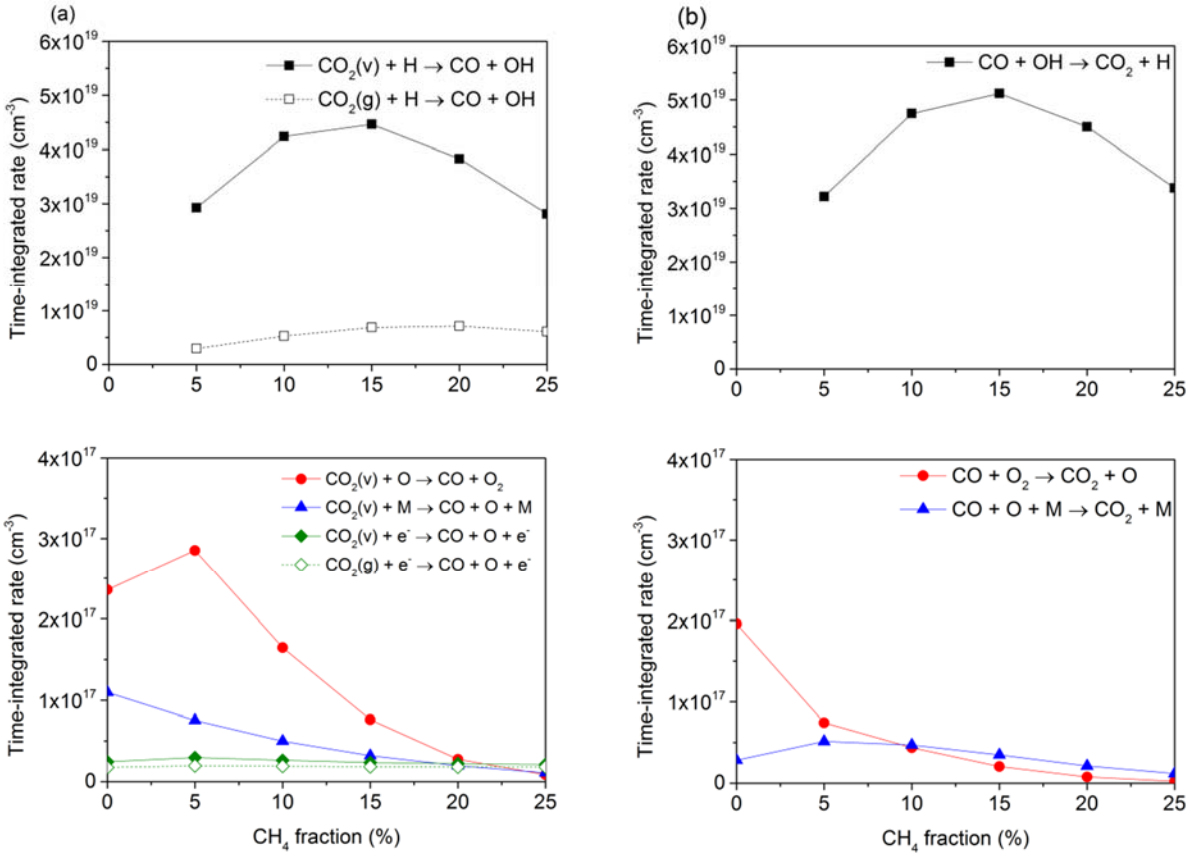

Figure S.4: Time-integrated rates of the most important loss (a) and formation (b) processes of CO_2, as a function of CH_4 fraction in the mixture.

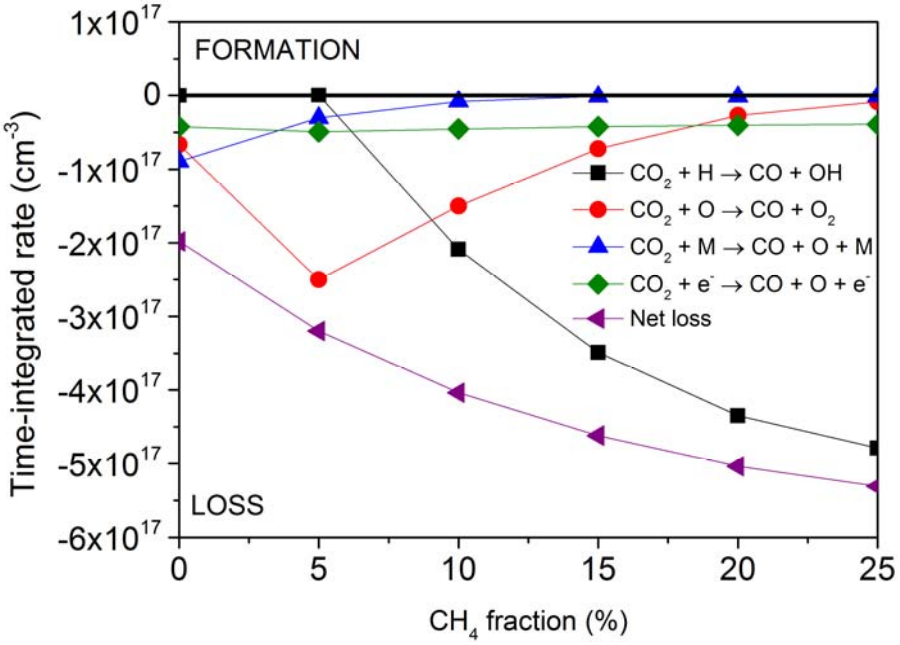

Figure S.5: Net time-integrated rates of the most important loss (and formation) processes of CO_2, as well as the total net loss rate, as a function of CH_4 fraction in the mixture. The loss processes are plotted with negative rates; the formation processes in principle with positive rates (but in this case, they are negligible).

Loss and formation of CH_4

Figure S.6 illustrates the time-integrated rates of the main loss (a) and formation (b) processes of CH_4. All the rates increase upon rising CH_4 fraction. The forward and backward reactions (i.e., loss and formation processes, respectively) are again plotted in the same color, for the sake of clarity. It is clear that for some loss rates, the backward reaction is (nearly) equally important, so we need to look again at the net rates, plotted in Figure S.7 (again in the same color). The reactions plotted as positive values contribute to the net formation of CH_4, while the reactions plotted as negative values again contribute to the net conversion (or loss) of CH_4. It is clear from Figure S.6 that some reactions yield a net formation of CH_4, especially the three-body reaction of CH_3 radicals with H atoms ($CH_3 + H + M \rightarrow CH_4 + M$), while other reactions give a net loss of CH_4, i.e., mainly the reaction of CH_4 molecules with OH or C_2H_3 radicals. The net CH_4 loss rate is also plotted. It rises with increasing CH_4 fraction, which explains why the overall (effective) CH_4 conversion indeed rises upon rising CH_4 fraction in the mixture, simply attributed to the rising CH_4 concentration.

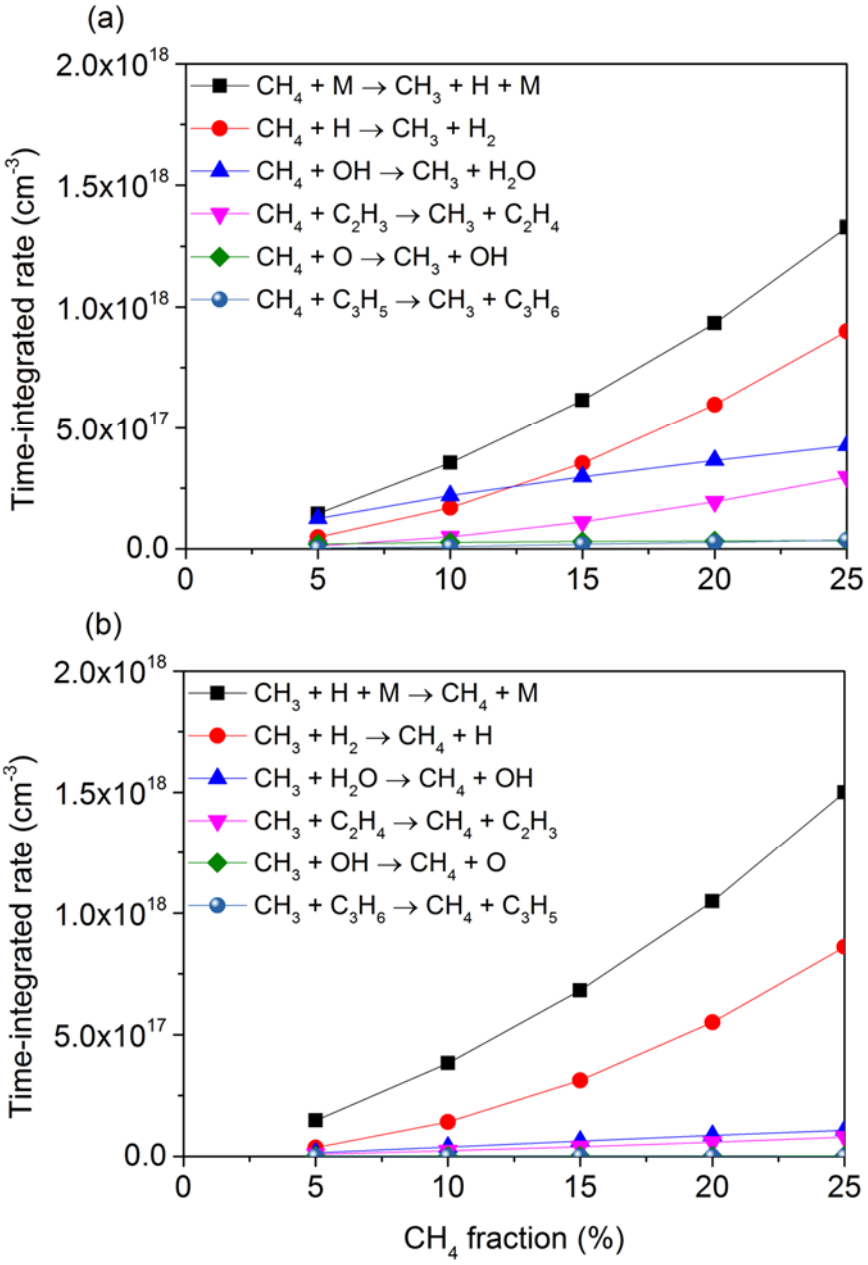

Figure S.6: Time-integrated rates of the most important loss (a) and formation (b) processes of CH_4, as a function of CH_4 fraction in the mixture.

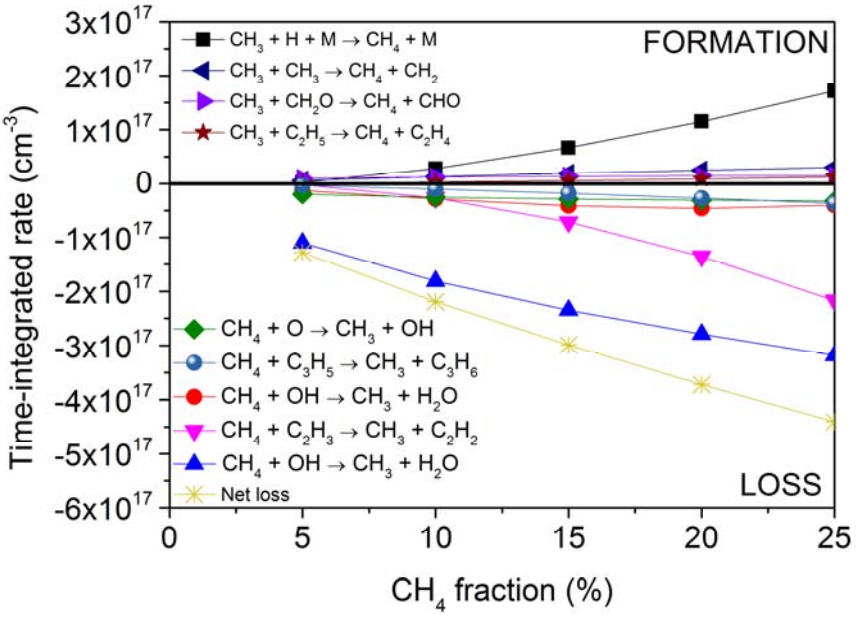

Figure S.7: Net time-integrated rates of the most important loss and formation processes of CH_4, as well as the total net loss rate, as a function of CH_4 fraction in the mixture. The loss processes are plotted with negative rates, while the formation processes are plotted with positive rates.

References

[1] N. Pinhão, A. Moura, J. B. Branco, J. Neves, *Int. J. Hydrogen Energy* **2016**, *41*, 9245–9255.

[2] S. Pancheshnyi, B. Eismann, G.J.M. Hagelaar, L.C. Pitchford, Computer code ZDPlasKin, http://www.zdplaskin.laplace.univ-tlse.fr (University of Toulouse, LAPLACE, CNRS-UPS-INP, Toulouse, France, 2008).

[3] J. M. Hagelaar, L. C. Pitchford, *Plasma Sources Sci. Technol. Plasma Sources Sci. Technol* **2005**, *14*, 722–733.

[4] A. Bogaerts, W. Wang, A. Berthelot, V. Guerra, *Plasma Sources Sci. Technol.* **2016**, *25*, 55016.

[5] M. Grofulović, L. L. Alves, V. Guerra, *J. Phys. D. Appl. Phys.* **2016**, *49*, 395207.

[6] C. De Bie, J. van Dijk, A. Bogaerts, *J. Phys. Chem. C* **2015**, *119*, 22331–22350.

[7] M. A. Lieberman, A. J. Lichtenberg, *Principles of Plasma Discharges and Materials Processing: Second Edition*, John Wiley & Sons, **2005**.

[8] G. Trenchev, S. Kolev, A. Bogaerts, *Plasma Sources Sci. Technol.* **2016**, *25*, 35014.

[9] R. Snoeckx, A. Bogaerts, *Chem. Soc. Rev.* in press.

[10] A. Fridman, *Plasma Chemistry*, Cambridge University Press, New York, **2008**.

[11] NIST Chemical Kinetics Database http://kinetics.nist.gov/kinetics/index.jsp (date: 27/02/2017).